

UC San Diego

UC San Diego Previously Published Works

Title

Cholinergic Neurotransmission Controls Orexigenic Endocannabinoid Signaling in the Gut in Diet-Induced Obesity.

Permalink

<https://escholarship.org/uc/item/06m8h7sm>

Journal

Journal of Neuroscience, 44(20)

ISSN

0270-6474

Authors

Wood, Courtney P

Alvarez, Camila

DiPatrizio, Nicholas V

Publication Date

2024-05-15

DOI

10.1523/jneurosci.0813-23.2024

Peer reviewed

The Journal of Neuroscience

<https://jneurosci.msubmit.net>

JN-RM-0813-23R1

Cholinergic neurotransmission controls orexigenic endocannabinoid signaling in the gut in diet-induced obesity

Nicholas DiPatrizio, University of California Riverside School of Medicine
Courtney Wood, University of California San Diego
Camila Alvarez, University of California Riverside

Commercial Interest:

Cholinergic neurotransmission controls orexigenic endocannabinoid signaling in the gut in diet-induced obesity

Abbreviated Title: Cholinergics drive eCB synthesis in obesity

Courtney P. Wood, Camila Alvarez, Nicholas V. DiPatrizio

Division of Biomedical Sciences, School of Medicine, University of California, Riverside, Riverside, CA, 92521, USA; University of California Riverside Center for Cannabinoid Research, Riverside, CA, 92521, USA

Corresponding Author: Nicholas V. DiPatrizio, ndipatri@medsch.ucr.edu

Number of Pages: 25

Number of Figures: 10

Number of Tables: 2

Number of Words for Abstract: 250

Number of Words for Introduction: 636

Number of Words for Discussion: 1,458

Conflict of Interest Statement: The authors declare no competing financial interests.

Acknowledgements: Research is funded by the National Institutes of Health (R01 DK119498 and L30 DK1149978) and the Tobacco-Related Disease Research Program (T29KT0232). The authors thank Samantha Sutley-Koury and Dr. Iryna Ethell's laboratory for their guidance in developing the cFos IHC assay, as well as Jeffrey Koury and Dr. Marcus Kaul's laboratory for training and use of the fluorescence microscope, and Will Cruz for assistance with chemical analyses.

1 **Abstract**

2 The brain bidirectionally communicates with the gut to control food intake and energy balance, which
3 becomes dysregulated in obesity. For example, endocannabinoid (eCB) signaling in the small-intestinal
4 epithelium (SI) is upregulated in diet-induced obese mice (DIO) and promotes overeating by a
5 mechanism that includes inhibiting gut-brain satiation signaling. Upstream neural and molecular
6 mechanism(s) involved in overproduction of orexigenic gut eCBs in DIO, however, are unknown. We
7 tested the hypothesis that overactive parasympathetic signaling at muscarinic acetylcholine receptors
8 (mAChRs) in the SI increases biosynthesis of the eCB, 2-arachidonoyl-*sn*-glycerol (2-AG), which drives
9 hyperphagia via local CB₁Rs in DIO. Male mice were maintained on a high-fat/high-sucrose western-style
10 diet for 60 days, then administered several mAChR antagonists 30 min prior tissue harvest or a food
11 intake test. Levels of 2-AG and activity of its metabolic enzymes in the SI were quantitated. DIO mice,
12 when compared to those fed a low-fat/no-sucrose diet, displayed increased expression of cFos protein
13 in the dorsal motor nucleus of the vagus, which suggests increased activity of efferent cholinergic
14 neurotransmission. These mice exhibited elevated levels of 2-AG biosynthesis in the SI, which was
15 reduced to control levels by mAChR antagonists. Moreover, the peripherally-restricted mAChR
16 antagonist, methylhomatropine bromide, and the peripherally-restricted CB₁R antagonist, AM6545,
17 reduced food intake in DIO mice for up to 24 h but had no effect in mice conditionally deficient in SI
18 CB₁Rs. These results suggest that hyperactivity at mAChRs in the periphery increases formation of 2-AG
19 in the SI and activates local CB₁Rs, which drives hyperphagia in DIO.

20

21

22

23

24

25 **Significance Statement**

26 Gut-brain signaling controls food intake and energy homeostasis; however, it is poorly
27 understood how gut-brain signaling becomes dysregulated in obesity. In this study, we demonstrated
28 that brain to gut communication is altered in obesity, leading to an increase in endocannabinoid
29 signaling in the GI tract, which drives overeating. Acutely blocking activity at muscarinic acetylcholine
30 receptors in the periphery attenuates intestinal endocannabinoid production and calorie intake in obese
31 animals. This effect was absent in mice conditionally lacking CB₁Rs in the intestinal epithelium. These
32 findings expand our understanding of the complex pathophysiology associated with obesity and
33 mechanisms of brain-gut-brain signaling.

34

35 **Introduction**

36 Food intake and energy balance are controlled by gut-brain neurotransmission, and this
37 communication becomes dysregulated in obesity (Berthoud, 2008; de Lartigue et al., 2011; de Lartigue
38 et al., 2014; Argueta et al., 2019; McDougle et al., 2021). For example, vagal afferent neurons in diet-
39 induced obese (DIO) mice displayed impaired responses to the satiation peptide, cholecystokinin (CCK)
40 (Daly et al., 2011), as well as reduced sensitivity to mechanical stimulation (Kentish et al., 2012) and
41 leptin signaling (de Lartigue et al., 2011). Mounting evidence also suggests that overactive
42 endocannabinoid (eCB) signaling in the upper small-intestinal lining in DIO mice (Artmann et al., 2008;
43 Izzo et al., 2009; Argueta and DiPatrizio, 2017) contributes to overeating and dysregulated gut brain-
44 mediated satiation by a mechanism that includes inhibiting nutrient-induced CCK release (Argueta et al.,
45 2019; DiPatrizio, 2021). Furthermore, recent studies highlight an important function for gut-brain
46 communication in the control of food preferences and reward (Han et al., 2018; Scalfani, 2018; Li et al.,

47 2022), and the contribution of gut-brain eCB signaling in these processes (DiPatrizio et al., 2013; Avalos
48 et al., 2020; Berland et al., 2022). Indeed, acute preferences for western-style high-fat/sucrose diets
49 versus low-fat/no-sucrose diets are absent in mice conditionally lacking cannabinoid subtype-1
50 receptors (CB₁Rs) in intestinal epithelial cells, which underscores an essential role for CB₁Rs in the
51 intestinal lining in gut-brain control of preferences for palatable foods (Avalos et al., 2020).

52 Less is known about how obesity affects activity of vagal efferent neurons, which provide dense
53 cholinergic innervation to the gastrointestinal tract from the caudal brainstem (Berthoud et al., 1991;
54 Altschuler et al., 1993). Nonetheless, early studies suggest that this parasympathetic neurotransmission
55 may play an important role in brain-gut signaling that controls feeding behavior. The peripherally-
56 restricted muscarinic acetylcholine receptor (mAChR) antagonist, atropine methyl nitrate, inhibited
57 intake of a liquid diet in sham-feeding rats (Lorenz et al., 1978) and prevented refeeding after a fast
58 (Pradhan and Roth, 1968). In addition, activity of cholinergic efferent vagal neurons that project from
59 the dorsal motor nucleus of the vagus (DMV) to the gut is controlled by central melanocortin-4
60 receptors (MC4Rs) (Sohn et al., 2013), which play a key role in energy homeostasis and attenuation of
61 food intake (Williams and Elmquist, 2012). Specific roles for the eCB system in brain-gut cholinergic
62 control of food intake and its dysregulation in obesity, however, are unclear.

63 Several reports suggest that mAChR signaling controls eCB production in the central nervous
64 system (Kim et al., 2002; Straiker and Mackie, 2007; Zhao and Tzounopoulos, 2011; Rinaldo and Hansel,
65 2013). Similarly, cholinergic signaling in the periphery stimulates biosynthesis of orexigenic eCBs in the
66 upper small-intestinal epithelium of fasted rats, an effect that was blunted by surgical resection of the
67 vagus nerve below the diaphragm or after administration of several mAChR antagonists (DiPatrizio et
68 al., 2015). Moreover, tasting dietary fats increased biosynthesis of eCBs in this organ and promoted
69 further intake of fat through activating local CB₁Rs (DiPatrizio et al., 2011; DiPatrizio et al., 2013). This
70 increased eCB activity was also blocked in vagotomized animals. Together, these studies suggest an

71 important role for the efferent vagus nerve in the biosynthesis of appetite-promoting eCBs in cells lining
72 the upper intestine.

73 A primary biosynthetic pathway for the abundant eCB, 2-arachidonoyl-*sn*-glycerol (2-AG),
74 requires a two-step enzymatic process that includes phospholipase C (PLC) and diacylglycerol lipase
75 (DGL) activity (Stella et al., 1997; Piomelli et al., 2007; Aaltonen et al., 2014). This pathway can be
76 activated by metabotropic receptors coupled to G_q-type g-proteins such as group I metabotropic
77 glutamate receptors or muscarinic acetylcholine receptor sub-types 1 and 3 (M₁ and M₃, respectively)
78 (Hulme et al., 1990; Caulfield and Birdsall, 1998; Jung et al., 2007; Aaltonen et al., 2014). Here, we tested
79 the hypothesis that overactive parasympathetic signaling at mAChRs increases biosynthesis of 2-AG in
80 the upper small-intestinal epithelium in DIO, which drives overeating via local CB₁Rs.

81

82 **Materials & Methods**

83 *Animals*

84 C57BL/6 male mice (Taconic, Oxnard, CA, USA) or transgenic mice (described below in
85 *Transgenic Mouse Generation*) 8-10 weeks of age were group-housed with *ad-libitum* access to standard
86 rodent laboratory diet (SD; Teklad 2020x, Envigo, Huntingdon, UK; 16% kcal from fat, 24% kcal from
87 protein, 60% kcal from carbohydrates) or Western Diet (WD; Research Diets D12709B, New Brunswick,
88 NJ, USA; 40% kcal from fat, 17% kcal from protein, 43% kcal from carbohydrates as mostly sucrose) and
89 water throughout all experiments unless otherwise stated. Mice were maintained on a 12-h dark/light
90 cycle beginning at 1800 h. All procedures met the U.S. National Institute of Health guidelines for care
91 and use of laboratory animals and were approved by the Institutional Animal Care and Use Committee
92 (IACUC) of the University of California, Riverside.

93 *Transgenic Mouse Generation*

94 Conditional intestinal epithelium-specific CB₁R-deficient mice (IntCB₁^{-/-}, Cnr1^{tm1.1 mrl}/vil-cre ERT2)
95 were generated by crossing Cnr1-floxed mice (IntCB₁^{+/+}, Cnr1^{tm1.1 mrl}; Taconic, Oxnard, CA, USA; Model
96 #7599) with Vil-CRE ERT2 mice donated by Dr. Randy Seeley (University of Michigan, Ann Arbor, MI,
97 USA) with permission from Dr. Sylvie Robin (Curie Institute, Paris, France). Cre recombinase expression
98 in the intestinal epithelium is driven by the villin promotor, which allows for conditional tamoxifen-
99 dependent Cre recombinase action to remove the *Cnr1* gene from these cells, as described by el Marjou
100 et al. (el Marjou et al., 2004). Cnr1^{tm1.1 mrl}/vil-cre ERT2 mice used in these experiments are referred to as
101 IntCB₁^{-/-}, and Cnr1^{tm1.1 mrl} control mice (lacking Cre recombinase) are referred to as IntCB₁^{+/+}. Tail snips
102 were collected from pups at weaning and DNA was extracted and analyzed by conventional PCR using
103 the following primers (5'-3'): GCAGGGATTATGTCCCTAGC (CNR1-ALT), CTGTTACCAGGAGTCTTAGC (1415-
104 35), GGCTCAAGGAATACTTATAACC (1415-37), GAACCTGATGGACATGTTTCAGG (vilcre, AA),
105 AGTGCGTTCGAACGCTAGAGCCTGT (vilcre, SS), TTACGTCCATCGTGG-ACAGC (vilcre, MYO F),
106 TGGGCTGGGTGTTAGCCTTA (vilcre, MYO R). Knockdown of Cnr1 expression in the intestinal epithelium
107 was verified by RT-qPCR immediately following feeding behavior experiments (intCB₁^{+/+} control mice,
108 1.000 ± 0.2869; intCB₁^{-/-} mice, 0.1226 ± 0.0149; $t_{(13)} = 3.282$, $p = 0.0060$ via two-tailed t-test).

109 *Drug Preparation and Administration*

110 IntCB₁^{-/-} and intCB₁^{+/+} mice were administered tamoxifen (IP, 40 mg per kg) daily for five
111 consecutive days. Tamoxifen (Sigma-Aldrich, St. Louis, MO, USA) was dissolved in corn oil using bath
112 sonication at a concentration of 10 mg per mL then stored at 37°C protected from light until
113 administration. Mice were group housed in disposable cages (14.7 x 9.2 x 5.5") at up to 5 mice per cage
114 throughout the injection period and for a 3-day post-injection period. JZL-184 (Tocris, Bristol, UK) was
115 incubated with intestinal epithelium tissue homogenate to inhibit MGL activity in the DGL enzyme

116 activity assay. The peripherally-restricted non-selective muscarinic acetylcholine receptor antagonist
117 methylhomatropine (bromide) (ATR; Cayman Chemicals, Ann Arbor, MI, USA) was dissolved in 0.9%
118 sterile sodium chloride solution (LabChem, Zelenople, PA, USA) and administered (IP, 2 mg per kg per 2
119 mL) 30 minutes prior to tissue harvest and testing. The selective muscarinic M₃ receptor antagonist DAU
120 5884 hydrochloride (DAU; Tocris Bioscience, Minneapolis, MN, USA) was dissolved in 0.9% sterile
121 sodium chloride solution (LabChem, Zelenople, PA, USA) and administered (IP, 2 mg per kg per 2 mL) 30
122 minutes prior to tissue harvest and testing. The selective muscarinic M₁ receptor antagonist Pirenzepine
123 dihydrochloride (PIR; Sigma-Aldrich, St. Louis, MO, USA) was dissolved in 0.9% sterile sodium chloride
124 solution (LabChem, Zelenople, PA, USA) and administered (IP, 2 mg per kg per 2 mL) 30 minutes prior to
125 tissue harvest and testing. The peripherally-restricted CB₁R neutral antagonist AM6545 (Northeastern
126 University Center for Drug Discovery, Boston, MA, USA) was administered (IP, 10 mg per kg per 2 mL) 30
127 minutes prior to testing. All antagonists were administered 30 minutes prior to testing to match
128 conditions of our previously published experiments (Argueta and DiPatrizio, 2017; Avalos et al., 2020).
129 The vehicle for AM6545 consisted of 7.5% dimethyl sulfoxide (DMSO, Sigma-Aldrich, St. Louis, MO, USA),
130 7.5% Tween 80 (Chem Implex Intl Inc., Wood Dale, IL, USA), and 85% 0.9% sterile sodium chloride
131 solution (LabChem, Zelenople, PA, USA).

132 *Lipid Extraction*

133 Animals were anesthetized with isoflurane at the time of tissue harvest (0900 h) following *ad*
134 *libitum* food and water access. Jejunum was quickly removed and washed in ice cold phosphate-
135 buffered saline (PBS), opened longitudinally on a stainless-steel tray on ice, and contents were removed.
136 Jejunum mucosa was isolated using glass slides to scrape epithelial layer and was snap-frozen in liquid
137 nitrogen (N₂). Samples were stored at -80°C until analysis. Frozen tissues were weighed and then
138 homogenized in 1 mL methanol (MeOH) solution containing 500 pmol [²H₅]-2-AG, 5 pmol [²H₄]-AEA, and
139 5 pmol [²H₄]-OEA or 500 pmol of dinonadecadienoin (19:2 diacylglycerol, 19:2 DAG; Nu-Check Prep,

140 Waterville, MN, USA) as internal standards. Lipids were extracted as previously described (Argueta and
141 DiPatrizio, 2017) and resuspended in 0.2 mL CHCl₃:MeOH (1:1). 1 µL of the resulting sample was
142 analyzed via ultra-performance liquid chromatography/tandem mass spectrometry (UPLC-MS/MS).

143 *LCMS Detection of 1-stearoyl, 2-arachidonoyl-sn-glycerol (SAG) and MAGs*

144 Data were acquired using an Acquity I Class UPLC with direct connection to a Xevo TQ-S Micro
145 Mass Spectrometer (Waters Corporation, Milford, MA, USA) with electrospray ionization (ESI) sample
146 delivery. 2-Arachidonoyl-*sn*-Glycerol (2-AG) and other analytes were detected as previously described
147 (Argueta et al., 2019). SAG was separated using an Acquity UPLC BEH C₁₈ column (2.1 mm x 50 mm i.d.,
148 1.7 µm, Waters Corporation), and eluted by a gradient of water, isopropyl alcohol (IPA), and acetonitrile
149 (ACN) containing 10 mM NH₄ formate at a flow rate of 0.4 mL per min and gradient: 80% ACN:water
150 (60:40) and 20% ACN:IPA (10:90) 0.5 min, 80% to 0% ACN:water 0.5 – 6.0 min, 0% ACN:water 6.0 – 6.25
151 min, 0% to 80% ACN:water 6.25 – 6.50 min. The column was maintained at 50°C, and samples were kept
152 at 10°C in accompanying sample manager. MS/MS detection was in positive ion mode with capillary
153 voltage maintained at 1.10 kV, and argon (99.998%) was used as collision gas. Cone voltages and
154 collision energies for respective analytes: SAG (18:0, 20:4) = 38v, 14v; 2-AG (20:4) = 30v, 12v; 2-OG
155 (18:1) = 42v, 10v; 2-DG (22:6) = 34v, 14v; 2-LG (18:2) = 30v, 10v; 19:2 DAG = 26v, 14v; [²H₅]-2-AG = 25v,
156 44v. Lipids were quantitated using a stable isotope dilution method detecting H⁺ or Na⁺ adducts of the
157 molecular ions [M + H/Na]⁺ in multiple reaction monitoring mode (MRM). Extracted ion chromatograms
158 for MRM transitions were used to quantitate analytes: SAG (*m/z* = 662.9 > 341.3), 2-AG (*m/z* = 379.3 >
159 287.3), 2-OG (*m/z* = 357.4 > 265.2), 2-DG (*m/z* = 403.3 > 311.2), 2-LG (*m/z* = 355.3 > 263.3), with 19:2
160 DAG (*m/z* = 662.9 > 627.5) as internal standard for SAG, and [²H₅]-2-AG (*m/z* = 384.3 > 93.4) as internal
161 standard for all MAGs. One “blank” sample that did not include any experimental tissue was processed
162 and analyzed in the same manner as all other samples. This control revealed no detectable eCBs and
163 related lipids included in our analysis.

164 *Enzyme Activity Assays*

165 Intestinal epithelium was collected as described above (*Lipid Extracts*) and approximately 100
166 mg of frozen tissue was homogenized in 2 mL of ice-cold 50 mM Tris-HCl, 320 mM sucrose (pH 7.5)
167 buffer, as previously described (Wiley et al., 2021). Homogenates were centrifuged at 800 g for 10 min
168 at 4°C and supernatant was collected. Protein supernatants were sonicated twice for 10 s and then
169 freeze-thawed in liquid N₂ twice. Samples were spun again, and supernatant protein content was
170 quantified using BCA assay and diluted to working concentration with Tris-HCl/sucrose buffer. For the
171 DGL activity assay, small-intestinal epithelial tissue homogenates (25 µg, room temperature) were
172 incubated with the MGL inhibitor, JZL-184 (0.3 µM; Tocris, Bristol, UK), and any other drugs tested for 10
173 minutes. Homogenates were then incubated in 0.2 mL Tris-HCl with 0.2% Triton X-100 (pH 7.0 at 37°C)
174 containing 20 nmol 19:2 DAG (Nu-Check Prep, Waterville, MN, USA) at 37°C for 30 min. Reactions were
175 stopped by adding 1 mL ice-cold methanol containing 25 pmol [²H₅]-2-AG as internal standard. Lipids
176 were extracted and the product of the reaction, monononadecadienoin (19:2 monoacylglycerol, 19:2
177 MAG), was analyzed via UPLC-MS/MS as previously described (Argueta et al., 2019). For the MGL activity
178 assay, small-intestinal epithelial tissue (10 µg) was incubated with 0.4 mL Tris-HCl with 0.1% bovine
179 serum albumin (BSA) (pH 8.0 at 37°C) containing 50 nmol 19:2 MAG (Nu-Check Prep, Waterville, MN,
180 USA; final volume 0.5 mL per reaction) at 37°C for 10 min. Reactions were stopped by adding 1 mL
181 MeOH containing 10 nmol heptadecanoic acid (17:1 free fatty acid, 17:1 FFA; Nu-Check Prep) as internal
182 standard. Lipids were extracted and the product of the reaction (19:2 free fatty acid, 19:2 FFA) was
183 analyzed via UPLC-MS/MS as previously described (Argueta et al., 2019). GraphPad Prism software
184 generated the following error message for the enzyme inhibition curves in **Figures 6B, C, and D**: *“For at*
185 *least one parameter, Prism was able to find a best-fit value but was unable to calculate a complete*
186 *confidence interval. This best-fit value should be interpreted with caution”*. Negative R² values are

187 indicative of no correlation between the drug concentration and enzyme activity, so we included this
188 information to further demonstrate that DAU, PIR, and ATR are not directly inhibiting DGL activity.

189 *Feeding Behavior*

190 Mice were single-housed in two-hopper feeding chambers (TSE Systems, Chesterfield, MO, USA)
191 for five days to acclimate, and received *ad-libitum* access to food and water throughout behavioral
192 testing. Total caloric intake of each diet (kcal), water intake (mL), and distance travelled (km) were
193 calculated every minute across the testing period, beginning at the start of the dark cycle (1800 h) for 24
194 h. Data were processed using TSE Phenomaster software, as previously described (Avalos et al., 2020).

195 *Gene Expression*

196 Total RNA from intestinal epithelium tissue was extracted using an RNeasy kit (Qiagen, Valencia,
197 CA, USA) and first-strand cDNA was generated using M-MLV reverse transcriptase (Invitrogen, Carlsbad,
198 CA, USA). Areas used for tissue collection and processing were sanitized with 70% ethanol solution then
199 treated with RNase inhibitor (RNase Out, G-Biosciences, St. Louis, MO, USA). Reverse transcription of
200 total RNA was performed as previously described (Argueta et al., 2019). Quantitative RT-PCR was
201 performed using preconfigured SYBR green PrimePCR assays (Biorad, Irvine, CA, USA) with the primer
202 for the CB₁R (Cnr1) gene transcript. Hprt was used as a housekeeping gene. Reactions were run in
203 duplicates and values expressed as relative mRNA expression.

204 *cFos Immunohistochemistry*

205 On the day of the experiment, mice were allowed *ad-libitum* access to food and water for the
206 entire day, and then fasted 30 minutes prior to the onset of the dark cycle (1730h) to reduce gut-brain
207 feedback resulting from food consumption. cFos protein can be detected 20-90 minutes following the
208 stimulus (Bullitt, 1990), therefore mice were perfused between 1845h and 1915h (45-75 minutes

209 following the onset of the dark period) to enable optimal cFos detection in the brainstem. Experiments
210 occurred in the absence of any drug or other treatment to examine whether DMV neuronal activation
211 differs between SD- and WD-fed mice in basal conditions. Animals were deeply anesthetized with
212 isoflurane and transcardially perfused with 40 mL of ice-cold PBS immediately followed by 40 mL of ice-
213 cold 4% paraformaldehyde (PFA). The brainstem was immediately collected and stored at 4°C overnight
214 in 4% PFA. Brainstems were transferred to a solution containing 30% sucrose and 0.01% sodium azide in
215 PBS and stored at 4°C until adequate cryopreservation was achieved (when tissue had completely sunk
216 to the bottom of the solution). Brainstems were stored in OCT compound at -20°C until processing. On
217 the day of the assay, 50 µM sections of the medulla were transferred to PBS and then sequentially
218 incubated (including PBS and/or PBST wash steps between incubations) in: 1) 10 mM citrate buffer, pH
219 6.0; 2) 4% normal goat serum (NGS) (Millipore Sigma, Burlington, MA, USA) in PBST; 3) anti-cFos rabbit
220 monoclonal antibody (1:500, Cell Signaling Technology, Danvers, MA, USA) or anti-ChAT monoclonal
221 antibody (1:500, Invitrogen, Carlsbad, CA, USA) in blocking buffer; 4) anti-rabbit IgG Alexa Fluor 488
222 conjugate (1:500, Cell Signaling Technology, Danvers, MA, USA) or donkey anti-IgG (H+L) Alexa Fluor 555
223 (1:500, Invitrogen, Carlsbad, CA, USA) in blocking buffer. Sections were mounted on glass slides,
224 allowed to air-dry overnight, and coverslips were added with VECTASHIELD mounting medium with DAPI
225 (Vector Laboratories, Newark, CA, USA) prior to imaging.

226 *Microscopy & Image Analysis*

227 Fluorescent images were taken on a Zeiss 200 M fluorescence deconvolution microscope
228 equipped with a computer-controlled stage and the appropriate filters for DAPI and FITC (Carl Zeiss
229 Microscopy GmbH, Jena, Germany). Slidebook software (version 6, Intelligent Imaging Innovations, Inc.,
230 Denver, CO) was used for all image acquisition. Quantitative analysis of cFos⁺ and ChAT⁺ cells in the DMV
231 was performed as described previously (Igelstrom et al., 2010; Perrin-Terrin et al., 2016). Briefly, one
232 section per animal was imaged at 10× so that local landmarks were visible to enable consistent analysis

233 between samples. The exposure period was kept the same for all analyzed images. Immunoreactivity
234 was quantified using Fiji open-source software (Schindelin et al., 2012). Images were subject to identical
235 black/white thresholding to enable counting of positive nuclei. Immunoreactive puncta were counted
236 using the Particle Analysis function within bilateral fixed areas of each image.

237 *Experimental Design & Statistical Analysis*

238 Details regarding the experimental design of individual experiments are provided in the figure
239 legends. Data were analyzed by GraphPad Prism version 9.5.0 (GraphPad Software, La Jolla, CA, USA)
240 using unpaired Student's *t*-tests (two-tailed), one-way ANOVA, two-way ANOVA, or three-way ANOVA
241 with Holm-Sidak's multiple comparisons *post-hoc* test when appropriate. Inhibition curves in **Figure 6**
242 were generated using a least squares fit of log[inhibitor] vs. normalized response. Results are expressed
243 as means \pm S.E.M. and significance was determined at $p < 0.05$.

244

245 **Results**

246 *Neuronal activity is increased in the DMV of DIO animals*

247 We tested the hypothesis that parasympathetic neurotransmission is overactive in DIO, which
248 drives overproduction of gut eCBs and associated hyperphagia. cFos⁺ cells in the dorsal motor nucleus of
249 the vagus (DMV) of untreated lean control mice fed SD (**Fig. 1A**) and DIO mice fed WD (**Fig. 1B**) were
250 quantified. WD-fed mice exhibited an increased number of cFos⁺ cells in the DMV when compared to SD-
251 fed controls, which suggests increased activity of DMV neurons in obesity (**Fig. 1C**). To confirm that the
252 hyperactive cells within the DMV of the mice fed WD were cholinergic, we quantified immunoreactivity
253 for cFos and choline acetyltransferase (ChAT, the biosynthetic enzyme for acetylcholine) in the DMV in a
254 second cohort of mice fed SD or WD. 73.73% of the cFos⁺ cells in the DMV of mice fed WD were also

255 immunoreactive for ChAT indicating that most hyperactive cells in the DMV are indeed cholinergic
256 (**Fig. 1D, G**). These mice not only exhibited an increased number of cFos⁺ cells in the DMV (**Fig. 1E**), but
257 also an increased number of cFos⁺ and ChAT⁺ dual-labeled cells in the DMV when compared mice fed SD
258 (**Fig. 1F**). Mice fed WD, when compared to those maintained on SD, also gained significantly more body
259 weight (**Fig. 2A**), demonstrated increased change in body weight (**Fig. 2B**), consumed more calories (**Fig.**
260 **2C**), and displayed increased epididymal fat mass (**Fig. 2D**), similar to previous studies (Argueta and
261 DiPatrizio, 2017; Argueta et al., 2019).

262

263 *mAChR antagonism normalizes eCB levels in the upper intestinal epithelium in DIO mice*

264 We next investigated whether pharmacological inhibition of mAChRs can block overactive eCB
265 production in the upper small-intestinal epithelium. Consistent with our previous findings (Argueta and
266 DiPatrizio, 2017; Argueta et al., 2019), mice fed WD exhibited higher levels of 2-AG in the upper small-
267 intestinal epithelium (**Fig. 3A**) when compared to SD control mice. WD mice treated with a single IP
268 injection of the selective M₃ mAChR antagonist, DAU (2 mg per kg), had significantly reduced levels of 2-
269 AG (**Fig. 3A**) and other monoacylglycerols (**Fig. 3B, C**) in the upper small-intestinal epithelium when
270 compared to vehicle-treated mice fed WD. Notably, levels were reduced to those found in SD mice.
271 Treatment with the selective M₁ mAChR antagonist, PIR (2 mg per kg), reduced levels of 2-AG in WD
272 mice when compared to vehicle; however, this effect was not significant for 2-AG (**Fig. 3A**) but was
273 significant for select other MAGs (**Fig. 3C**). Given this result, we performed a dose-response analysis to
274 examine the effects of several doses of PIR within a log step of 2 mg per kg on MAG levels in the small-
275 intestinal epithelium of WD-fed mice (**Fig. 4A-D**, doses of 0.0, 0.65, 2.0, and 6.5 mg per kg). PIR at 2.0 mg
276 per kg, but not 0.65 or 6.5 mg per kg, significantly reduced levels of 2-AG (**Fig. 4A**) and select other
277 MAGs (**Fig. 4B**) in the small-intestinal epithelium. Lastly, the peripherally-restricted non-selective mAChR

278 antagonist, ATR (2 mg per kg), reduced levels of 2-AG (**Fig. 3A**) and select other MAGs (**Fig. 3B**) in mice
279 fed WD to levels found in mice fed SD.

280

281 *SAG formation and DGL activity in jejunum mucosa are inhibited by mAChR antagonism*

282 We next tested if changes in metabolism of monoacylglycerols (see **Fig. 5D**) in the upper small-
283 intestinal epithelium led to increased levels of 2-AG in WD mice and the ability for mAChR antagonists to
284 normalize levels to those found in SD control mice. We first analyzed levels of the diacylglycerol
285 precursor of 2-AG, 1-stearoyl,2-arachidonoyl-*sn*-glycerol (SAG). Like 2-AG, levels of SAG were
286 significantly elevated in the intestinal epithelium of vehicle-treated WD mice when compared to vehicle-
287 treated SD mice, and treatment with DAU (2 mg per kg), PIR (2 mg per kg), and ATR (2 mg per kg)
288 reduced SAG levels in WD mice to those found in SD mice (**Fig. 5A**). Furthermore, activity of
289 diacylglycerol lipase (DGL) – an eCB biosynthetic enzyme responsible for the hydrolysis of SAG and its
290 conversion to 2-AG – was similarly reduced by treatment with mAChR antagonists (**Fig. 5B**). Activity of
291 monoacylglycerol lipase (MGL), a primary degradative enzyme responsible for 2-AG inactivation (Dinh et
292 al., 2002) was not significantly affected by drug treatments (**Fig. 5C**).

293

294 *Anticholinergics do not affect 2-AG metabolic enzyme activity ex vivo*

295 We utilized our UPLC/MS²-based DGL activity assay (Wiley et al., 2021) to confirm that DGL
296 activity was not directly disrupted *ex vivo* by any of the drugs used *in vivo*. Activity of DGL in intestinal
297 epithelium tissue from WD mice was inhibited in a concentration-dependent manner by an inhibitor of
298 DGL, tetrahydrolipstatin (THL, 3nM to 1µM range) (**Fig. 6A**). In contrast to THL, incubation of tissue with
299 a wide range of concentrations of mAChR antagonists used in these studies including ATR (**Fig. 6B**, 10nM

300 to 10 μ M range), DAU (**Fig. 6C**, 10nM to 100 μ M range), and PIR (**Fig. 6D**, 10nM to 10 μ M range) failed to
301 affect enzymatic activity of DGL, which suggests that these drugs do not directly interfere with DGL
302 activity.

303

304 *mAChR antagonism reduces caloric intake in DIO mice*

305 Roles for peripheral mAChRs and CB₁Rs in overeating were evaluated next in mice fed WD. A
306 single dose of ATR (2mg per kg) reduced caloric intake for up to 24 h in WD mice (**Fig. 7A**) but had no
307 effect in SD mice (**Fig. 7B**). Moreover, ATR treatment in WD mice reduced caloric intake to similar levels
308 induced by the peripherally-restricted CB₁R antagonist, AM6545 (**Fig. 7A**, 10 mg/kg). When ATR and
309 AM6545 were co-administered in WD mice, caloric intake was comparable to intakes found after
310 administration of each drug alone (**Fig. 7A**). Treatment with AM6545 alone or in combination with ATR
311 did not significantly affect intake in SD mice (**Fig. 7B**). A single injection of DAU (2mg per kg) also caused
312 a reduction in caloric intake in WD mice – but not SD mice – for up to 12 h (**Fig. 7C, 7D**). In contrast to
313 DAU and ATR, PIR (2mg per kg) had no effect on intake irrespective of diet (**Fig. 7E, 7F**). ATR and
314 AM6545 each had a minor effect on ambulation in mice fed WD (**Fig. 8A**), while ATR and AM65645 in
315 combination reduced ambulation in both mice fed WD and in lean mice (**Fig. 8A, 8C**, respectively, and
316 accompanying **Table 1**). DAU did not impact ambulation but did have an overall effect on water intake in
317 WD mice (**Fig. 8E, 8F, respectively**, and accompanying **Table 1**), which may be a result of reduced food
318 intake (**Fig. 7C**). PIR at 2 mg per kg had no effect on water intake or ambulation in WD or SD mice (**Fig.**
319 **8I, 8J, 8K, 8L**).

320 Based on our findings from the biochemical dose response analysis of PIR (**Fig. 4A-D**), we aimed
321 to examine the effects of the same doses of PIR on food intake, water intake, and ambulation. PIR did
322 not significantly affect water intake (**Fig. 4F**) or ambulation (**Fig. 4G**) in WD-fed animals at any of the

323 doses tested (0.0, 0.65, 2.0, 6.5 mg per kg). A mild main effect of dose on food intake was observed (**Fig.**
324 **4E**, $p=0.02$ for dose by 2-way ANOVA); however, no significant differences were detected between doses
325 in a *post-hoc* multiple comparisons analysis.

326

327 *Inhibiting peripheral CB₁Rs or mAChRs failed to affect food intake in mice conditionally lacking CB₁Rs in*
328 *the intestinal epithelium*

329 We next utilized conditional intestinal epithelium-specific CB₁R-deficient mice [intCB₁^{-/-} (Avalos
330 et al., 2020; Wiley and DiPatrizio, 2022)] to determine if CB₁Rs in intestinal epithelial cells were required
331 for the appetite-suppressing effects of peripherally-restricted CB₁R and mAChR antagonists in obese WD
332 mice. IntCB₁^{-/-} mice and control mice with functional CB₁Rs in the intestinal epithelium (intCB₁^{+/+}) were
333 placed on WD for 60 days. AM6545 (10 mg/kg) or ATR (2 mg/kg) treatment reduced caloric intake for up
334 to 24 hours in WD intCB₁^{+/+} control mice (**Fig. 9A**). Notably, however, neither drug had an effect on
335 intake in WD intCB₁^{-/-} mice (**Fig. 9B**). Both intCB₁^{+/+} and intCB₁^{-/-} mice had largely similar body weights
336 throughout diet exposure (**Fig. 9C**); however, analysis of change in body weight from baseline by two-
337 way ANOVA revealed a genotype effect that indicated intCB₁^{-/-} mice had lower body weight gain when
338 compared to intCB₁^{+/+} control mice (**Fig. 9D**). Independently, AM6545 reduced ambulation in intCB₁^{+/+}
339 mice, but had no effect on ambulation in intCB₁^{-/-} animals (**Fig. 10A, C** and **Table 2**). ATR also yielded a
340 minor effect on ambulation in IntCB₁^{+/+} mice (**Fig. 10A**). AM6545 reduced water intake in intCB₁^{-/-} mice
341 but did not affect water intake in intCB₁^{+/+} mice (**Fig. 10B, D** and accompanying **Table 2**).

342

343 **Discussion**

344 We report that (i) cholinergic neuronal activity in the DMV of DIO mice is increased when
345 compared lean mice, (ii) cholinergic activity at peripheral mAChRs in DIO promotes biosynthesis of 2-AG
346 in the upper-intestinal epithelium by a mechanism that includes increased production of local 2-AG
347 precursors and their conversion to 2-AG, and (iii) CB₁Rs in the intestinal epithelium are required for
348 hyperphagia associated with overstimulation of these pathways in DIO. These results suggest a novel
349 brain-gut mechanism that drives overeating in DIO through interactions between cholinergic
350 neurotransmission and orexigenic eCB signaling in the gut.

351 DIO mice, when compared to lean controls, displayed a significantly larger number of cFos⁺ and
352 dual-labeled cFos⁺ ChAT⁺ cells in the DMV, which suggests increased activity of efferent parasympathetic
353 vagal fibers. The DMV is the primary source of parasympathetic input to the digestive system (Gibbons,
354 2019); indeed, over 70% of the cFos⁺ cells in the DMV of the WD-fed mice were shown to be
355 immunoreactive for ChAT. Though it is likely that these overactive cholinergic cells in the DMV are the
356 source of increased parasympathetic activity in the GI tract of the obese mice, motor neurons
357 originating in the DMV have functionally and anatomically discrete outputs to distinct segments of the
358 gastrointestinal tract and other organs (Rogers et al., 2006; Schubert and Peura, 2008; Mawe et al.,
359 2018; Tao et al., 2021). Future experiments will be necessary to further confirm if the same DMV
360 neurons that are activated in obese mice are the source of mAChR hyperactivity that leads to
361 overproduction of 2-AG in the upper small-intestinal epithelium.

362 Although not quantified, an increase in the number of cFos⁺ cells in other regions of the
363 intermediate medulla, namely the nucleus of the solitary tract (NTS), were observed. Thus, it is possible
364 that a general dysregulation within the medulla of obese mice occurs. Accordingly, it was recently
365 reported that the daily rhythms of oscillating cells within the NTS are disrupted by exposure to high-fat
366 diet (Chrobok et al., 2022b). The same group also demonstrated that high-fat diet exposure amplified
367 the daily variation of time-keeping cells within the DMV and blunted neuronal responsiveness to

368 metabolic neuromodulators (Chrobok et al., 2022a). These studies and others (Kentish et al., 2012;
369 Kentish et al., 2016; Clyburn et al., 2018; Zhang et al., 2020; Kovacs and Hajnal, 2022) support the notion
370 that select brainstem nuclei, which are responsible for sensing nutritional status and maintaining
371 metabolic homeostasis (i.e., DMV and NTS), become dysregulated in response to metabolic challenges.

372 Our data reveal a key role for peripheral mAChRs in controlling eCB biosynthesis in the intestinal
373 epithelium in DIO mice. These animals had elevated levels of (i) the 2-AG precursor, SAG, (ii) activity of
374 the biosynthetic enzyme for 2-AG and other MAGs, DGL, and (iii) 2-AG in the intestinal epithelium, which
375 was all attenuated by treatment with the M₃-selective antagonist, DAU, or the non-selective
376 peripherally-restricted mAChR antagonist, ATR. Moreover, the M₁-selective antagonist, PIR, was
377 effective at reducing both SAG and DGL activity levels; however, it only significantly reduced 2-AG levels
378 in the follow-up dose response experiment at the 2.0 mg per kg dose, but not 0.65 or 6.5 mg per kg
379 (**Fig.4A**). It is notable that while M₁ antagonism did influence MAG formation within the intestinal
380 epithelium, it did not significantly affect feeding behavior at any dose tested. Together, these results
381 suggest a more prominent role for the M₃ mAChR subtype in driving eCB biosynthesis and overeating in
382 DIO, and also highlight the necessity for future experiments exploring roles for M₁ versus M₃ mAChRs in
383 food intake and related behaviors. Furthermore, we reported that following 24 hr of food deprivation
384 (another metabolic challenge that has been shown to elevate intestinal 2-AG), DAU – but not PIR –
385 blocked biosynthesis of 2-AG in the upper small-intestinal epithelium of rats (DiPatrizio et al., 2015). In
386 addition, M₃ mAChR activation in the central nervous system initiates a signaling cascade that rapidly
387 upregulates expression of Cnr1 mRNA and potentiates responses to CB₁R agonists, such as 2-AG (Marini
388 et al., 2023). Given that mRNA for both M₁ and M₃ subtypes is expressed in mouse duodenum, jejunum,
389 and ileum epithelial cells (Muise et al., 2017), future studies should determine the expression patterns
390 of these receptors in specific cell types and their co-localization with eCB metabolic enzymes and CB₁Rs
391 throughout the gastrointestinal tract.

392 Our results suggest that pharmacological inhibition of peripheral M₃ mAChRs – alone or in
393 combination with inhibitors of peripheral CB₁Rs – could be beneficial for reducing caloric intake in
394 human obesity. This therapeutic strategy, however, may be met with deleterious side effects. For
395 example, ATR alone or in combination with AM6545 led to reductions in ambulation (**Figures 8A, C,**
396 **10A**). In addition, Cluny *et al.* reported that blocking peripheral CB₁Rs with daily injections of AM6545
397 did not cause malaise in rodents (Cluny *et al.*, 2010); however, it is possible that ATR and AM6545 in
398 combination may generate unfavorable effects. It should also be noted that M₃ mAChR antagonism may
399 lead to a reduction in insulin secretion by pancreatic β -cells (Ruiz de Azua *et al.*, 2011) and glucagon
400 secretion by α -cells (Duttaroy *et al.*, 2004), thereby suppressing the anorectic effect of these hormones
401 and allowing feeding to return to baseline levels prematurely in the DAU-treated animals in our study
402 (**Figure 7C**). An additional concern associated with the therapeutic use of ATR is the role for M₂ mAChRs
403 in the regulation of cardiac function (Peter *et al.*, 2005). Cardiac function was not measured in the
404 current study, but if ATR or related drugs are to be investigated for their potential as a treatment for
405 obesity, possible cardiac side-effects must be considered.

406 The eCB system plays a critical role in the seeking and sensing of calorie-dense foods (DiPatrizio
407 and Piomelli, 2012). Indeed, we reported a role for intestinal CB₁Rs in preferences for WD (Avalos *et al.*,
408 2020). In these studies, mice treated with the CB₁R inverse agonist, AM251, displayed no preference for
409 the highly palatable WD for up to 3 h. In addition, preferences for WD were largely abolished for up to 6
410 hours in mice conditionally lacking CB₁Rs in the intestinal epithelium. Notably, preferences for the WD
411 returned by 24 h after initiation of the preference test in these mice. These findings suggest that (i)
412 CB₁Rs in the intestinal epithelium are essential for acute preferences for high-fat, high-sugar foods and
413 (ii) other biochemical mechanisms may override eCB control of food preferences over time and should
414 be evaluated in the future (Avalos *et al.*, 2020).

415 The eCB system also directly and indirectly interacts with afferent vagal signaling to control food
416 intake, which becomes dysregulated in DIO (Argueta et al., 2019; Christie et al., 2020c; Christie et al.,
417 2020a, b; DiPatrizio, 2021; Berland et al., 2022). For example, CB₁Rs are expressed in enteroendocrine I
418 cells in the intestinal epithelium (Sykaras et al., 2012; Argueta et al., 2019). In response to nutrients
419 entering the lumen, these cells produce and secrete the satiation peptide, CCK, which induces satiation
420 via interactions with CCK_A receptors on afferent vagal fibers (Clemmensen et al., 2017). We reported
421 that elevated levels of 2-AG in the small-intestinal epithelium of DIO mice inhibits gut-brain satiation
422 signaling by a mechanism that includes blocking nutrient-induced release of CCK (Argueta et al., 2019).
423 This effect was reversed by the peripheral CB₁R antagonist, AM6545, which restored the ability for
424 nutrients to induce CCK release. Moreover, the hypophagic effects of AM6545 were completely reversed
425 by a CCK_A antagonist in DIO mice. Together, these data suggest that in DIO, overactive eCB signaling at
426 CB₁Rs on I cells in the upper-intestinal lining inhibits nutrient-induced CCK release, which may reduce
427 activity of vagal afferent neurons and allow DIO mice to continue feeding past satiation. A direct test of
428 this hypothesis, however, remains for future experiments. Future studies should also examine whether
429 ATR treatment is reducing caloric intake in DIO mice via a similar CCK-mediated mechanism. While this
430 work is yet to be completed, participation of the afferent vagus nerve in these processes is likely.
431 Accordingly, multiple studies have revealed the necessity of intact vagal afferent signaling for preventing
432 hyperphagia and weight gain, particularly in DIO (Covasa and Ritter, 1998; Daly et al., 2011; Kentish et
433 al., 2012; de Lartigue et al., 2014; McDougale et al., 2021). In addition, recent studies identified a
434 specialized subset of enteroendocrine cells lining the intestine that detect nutrients and communicate
435 with vagal afferent fibers via functional synapses (Kaelberer et al., 2018; Kaelberer et al., 2020). Studies
436 examining whether CB₁Rs also control neuropod activity in these processes and may become
437 dysregulated in DIO remain to be performed.

438 In summary, our results identify a previously undescribed brain-gut pathway that recruits
439 cholinergic signaling to drive eCB-mediated overeating in DIO. Components of this pathway may be
440 targets for anti-obesity therapeutics.

441

442 **References**

- 443 Aaltonen N, Riera Ribas C, Lehtonen M, Savinainen JR, Laitinen JT (2014) Brain regional cannabinoid
444 CB(1) receptor signalling and alternative enzymatic pathways for 2-arachidonoylglycerol
445 generation in brain sections of diacylglycerol lipase deficient mice. *Eur J Pharm Sci* 51:87-95.
- 446 Altschuler S, Escardo J, Lynn R, Miselis R (1993) The Central Organization of the Vagus Nerve Innervating
447 the Colon of the Rat. In, pp 502-509. *Gastroenterology*.
- 448 Argueta D, DiPatrizio N (2017) Peripheral endocannabinoid signaling controls hyperphagia in western
449 diet-induced obesity. *Physiology & Behavior* 171:32-39.
- 450 Argueta D, Perez P, Makriyannis A, DiPatrizio N (2019) Cannabinoid CB1 Receptors Inhibit Gut-Brain
451 Satiety Signaling in Diet-Induced Obesity. *Frontiers in Physiology* 10.
- 452 Artmann A, Petersen G, Hellgren LI, Boberg J, Skonberg C, Nellemann C, Hansen SH, Hansen HS (2008)
453 Influence of dietary fatty acids on endocannabinoid and N-acyl ethanolamine levels in rat brain,
454 liver and small intestine. *Biochim Biophys Acta* 1781:200-212.
- 455 Avalos B, Argueta D, Perez P, Wiley M, Wood C, DiPatrizio N (2020) Cannabinoid CB1 Receptors in the
456 Intestinal Epithelium Are Required for Acute Western-Diet Preferences in Mice. *Nutrients* 12.
- 457 Berland C, Castel J, Terrasi R, Montalban E, Foppen E, Martin C, Muccioli GG, Luquet S, Gangarossa G
458 (2022) Identification of an endocannabinoid gut-brain vagal mechanism controlling food reward
459 and energy homeostasis. *Mol Psychiatry* 27:2340-2354.
- 460 Berthoud H, Carlson N, Powley T (1991) Topography of Efferent Vagal Innervation of the Rat
461 Gastrointestinal-Tract. *American Journal of Physiology* 260:R200-R207.
- 462 Berthoud HR (2008) The vagus nerve, food intake and obesity. *Regul Pept* 149:15-25.
- 463 Bullitt E (1990) Expression of C-Fos-Like Protein as a Marker for Neuronal-Activity Following Noxious-
464 Stimulation in the Rat. *Journal of Comparative Neurology* 296:517-530.
- 465 Caulfield MP, Birdsall NJ (1998) International Union of Pharmacology. XVII. Classification of muscarinic
466 acetylcholine receptors. *Pharmacol Rev* 50:279-290.
- 467 Christie S, O'Rielly R, Li H, Wittert GA, Page AJ (2020a) Biphasic effects of methanandamide on murine
468 gastric vagal afferent mechanosensitivity. *The Journal of physiology* 598:139-150.
- 469 Christie S, O'Rielly R, Li H, Wittert GA, Page AJ (2020b) High fat diet induced obesity alters
470 endocannabinoid and ghrelin mediated regulation of components of the endocannabinoid
471 system in nodose ganglia. *Peptides* 131:170371.
- 472 Christie S, O'Rielly R, Li H, Nunez-Salces M, Wittert GA, Page AJ (2020c) Modulatory effect of
473 methanandamide on gastric vagal afferent satiety signals depends on nutritional status. *The*
474 *Journal of physiology* 598:2169-2182.
- 475 Chrobok L, Klich JD, Jeczmiem-Lazur JS, Pradel K, Palus-Chramiec K, Sanetra AM, Piggins HD,
476 Lewandowski MH (2022a) Daily changes in neuronal activities of the dorsal motor nucleus of the
477 vagus under standard and high-fat diet. *J Physiol* 600:733-749.
- 478 Chrobok L, Klich JD, Sanetra AM, Jeczmiem-Lazur JS, Pradel K, Palus-Chramiec K, Kepczynski M, Piggins
479 HD, Lewandowski MH (2022b) Rhythmic neuronal activities of the rat nucleus of the solitary

480 tract are impaired by high-fat diet - implications for daily control of satiety. *J Physiol* 600:751-
481 767.

482 Clemmensen C, Muller TD, Woods SC, Berthoud HR, Seeley RJ, Tschop MH (2017) Gut-Brain Cross-Talk in
483 Metabolic Control. *Cell* 168:758-774.

484 Cluny NL, Vemuri VK, Chambers AP, Limebeer CL, Bedard H, Wood JT, Lutz B, Zimmer A, Parker LA,
485 Makriyannis A, Sharkey KA (2010) A novel peripherally restricted cannabinoid receptor
486 antagonist, AM6545, reduces food intake and body weight, but does not cause malaise, in
487 rodents. *Br J Pharmacol* 161:629-642.

488 Clyburn C, Travagli R, Browning K (2018) Acute high-fat diet upregulates glutamatergic signaling in the
489 dorsal motor nucleus of the vagus. *American Journal of Physiology-Gastrointestinal and Liver
490 Physiology* 314:G623-G634.

491 Covasa M, Ritter RC (1998) Rats maintained on high-fat diets exhibit reduced satiety in response to CCK
492 and bombesin. *Peptides* 19:1407-1415.

493 Daly DM, Park SJ, Valinsky WC, Beyak MJ (2011) Impaired intestinal afferent nerve satiety signalling and
494 vagal afferent excitability in diet induced obesity in the mouse. *J Physiol* 589:2857-2870.

495 de Lartigue G, Ronveaux CC, Raybould HE (2014) Deletion of leptin signaling in vagal afferent neurons
496 results in hyperphagia and obesity. *Mol Metab* 3:595-607.

497 de Lartigue G, de la Serre C, Espero E, Lee J, Raybould H (2011) Diet-induced obesity leads to the
498 development of leptin resistance in vagal afferent neurons. *American Journal of Physiology-
499 Endocrinology and Metabolism* 301:E187-E195.

500 Dinh TP, Carpenter D, Leslie FM, Freund TF, Katona I, Sensi SL, Kathuria S, Piomelli D (2002) Brain
501 monoglyceride lipase participating in endocannabinoid inactivation. *Proceedings of the National
502 Academy of Sciences of the United States of America* 99:10819-10824.

503 DiPatrizio NV (2021) Endocannabinoids and the Gut-Brain Control of Food Intake and Obesity. *Nutrients*
504 13.

505 DiPatrizio NV, Piomelli D (2012) The thrifty lipids: endocannabinoids and the neural control of energy
506 conservation. *Trends Neurosci* 35:403-411.

507 DiPatrizio NV, Joslin A, Jung KM, Piomelli D (2013) Endocannabinoid signaling in the gut mediates
508 preference for dietary unsaturated fats. *Faseb J* 27:2513-2520.

509 DiPatrizio NV, Astarita G, Schwartz G, Li X, Piomelli D (2011) Endocannabinoid signal in the gut controls
510 dietary fat intake. *Proceedings of the National Academy of Sciences of the United States of
511 America* 108:12904-12908.

512 DiPatrizio NV, Igarashi M, Narayanaswami V, Murray C, Gancayco J, Russell A, Jung KM, Piomelli D (2015)
513 Fasting stimulates 2-AG biosynthesis in the small intestine: role of cholinergic pathways. *Am J
514 Physiol Regul Integr Comp Physiol* 309:R805-813.

515 Duttaroy A, Zimlik CL, Gautam D, Cui Y, Mears D, Wess J (2004) Muscarinic stimulation of pancreatic
516 insulin and glucagon release is abolished in m3 muscarinic acetylcholine receptor-deficient mice.
517 *Diabetes* 53:1714-1720.

518 el Marjou F, Janssen KP, Chang BH, Li M, Hindie V, Chan L, Louvard D, Chambon P, Metzger D, Robine S
519 (2004) Tissue-specific and inducible Cre-mediated recombination in the gut epithelium. *Genesis*
520 39:186-193.

521 Gibbons CH (2019) Chapter 27 - Basics of autonomic nervous system function. In: *Handbook of Clinical
522 Neurology* (Aminoff MJ, Boller F, Swaab DF, eds), pp 407-418: Elsevier.

523 Han W, Tellez LA, Perkins MH, Perez IO, Qu T, Ferreira J, Ferreira TL, Quinn D, Liu ZW, Gao XB, Kaelberer
524 MM, Bohórquez DV, Shammah-Lagnado SJ, de Lartigue G, de Araujo IE (2018) A Neural Circuit
525 for Gut-Induced Reward. *Cell* 175:887-888.

526 Hulme EC, Birdsall NJ, Buckley NJ (1990) Muscarinic receptor subtypes. *Annu Rev Pharmacol Toxicol*
527 30:633-673.

528 Igelstrom K, Herbison A, Hyland B (2010) ENHANCED c-Fos EXPRESSION IN SUPERIOR COLLICULUS,
529 PARAVENTRICULAR THALAMUS AND SEPTUM DURING LEARNING OF CUE-REWARD
530 ASSOCIATION. *Neuroscience* 168:706-714.

531 Izzo A, Piscitelli F, Capasso R, Aviello G, Romano B, Borrelli F, Petrosino S, Di Marzo V (2009) Peripheral
532 endocannabinoid dysregulation in obesity: relation to intestinal motility and energy processing
533 induced by food deprivation and re-feeding. *British Journal of Pharmacology* 158:451-461.

534 Jung KM, Astarita G, Zhu C, Wallace M, Mackie K, Piomelli D (2007) A key role for diacylglycerol lipase-
535 alpha in metabotropic glutamate receptor-dependent endocannabinoid mobilization. *Mol*
536 *Pharmacol* 72:612-621.

537 Kaelberer MM, Rupprecht LE, Liu WW, Weng P, Bohorquez DV (2020) Neuropod Cells: The Emerging
538 Biology of Gut-Brain Sensory Transduction. *Annual review of neuroscience* 43:337-353.

539 Kaelberer MM, Buchanan KL, Klein ME, Barth BB, Montoya MM, Shen X, Bohorquez DV (2018) A gut-
540 brain neural circuit for nutrient sensory transduction. *Science* 361.

541 Kentish S, Vincent A, Kennaway D, Wittert G, Page A (2016) High-Fat Diet-Induced Obesity Ablates
542 Gastric Vagal Afferent Circadian Rhythms. *Journal of Neuroscience* 36:3199-3207.

543 Kentish S, Li H, Philp L, O'Donnell T, Isaacs N, Young R, Wittert G, Blackshaw L, Page A (2012) Diet-
544 induced adaptation of vagal afferent function. *Journal of Physiology-London* 590:209-221.

545 Kim J, Isokawa M, Ledent C, Alger BE (2002) Activation of muscarinic acetylcholine receptors enhances
546 the release of endogenous cannabinoids in the hippocampus. *J Neurosci* 22:10182-10191.

547 Kovacs P, Hajnal A (2022) Short-term high-fat diet consumption increases body weight and body
548 adiposity and alters brain stem taste information processing in rats. *Chemical Senses* 47.

549 Li M, Tan HE, Lu Z, Tsang KS, Chung AJ, Zuker CS (2022) Gut-brain circuits for fat preference. *Nature*
550 610:722-730.

551 Lorenz D, Nardi P, Smith GP (1978) Atropine methyl nitrate inhibits sham feeding in the rat. *Pharmacol*
552 *Biochem Behav* 8:405-407.

553 Marini P, Cowie P, Ayar A, Bewick GS, Barrow J, Pertwee RG, MacKenzie A, Tucci P (2023) M3 Receptor
554 Pathway Stimulates Rapid Transcription of the CB1 Receptor Activation through Calcium
555 Signalling and the CNR1 Gene Promoter. *Int J Mol Sci* 24.

556 Mawe G, Lavoie B, Nelson M, Pozo M (2018) Neuromuscular Function in the Biliary Tract. In: *Physiology*
557 *of the Gastrointestinal Tract* (Said H, ed), pp 453-468: Elsevier/Academic Press.

558 McDougale M, Quinn D, Diepenbroek C, Singh A, de la Serre C, de Lartigue G (2021) Intact vagal gut-brain
559 signalling prevents hyperphagia and excessive weight gain in response to high-fat high-sugar
560 diet. *Acta Physiol (Oxf)* 231:e13530.

561 Muise ED, Gandotra N, Tackett JJ, Bamdad MC, Cowles RA (2017) Distribution of muscarinic
562 acetylcholine receptor subtypes in the murine small intestine. *Life sciences* 169:6-10.

563 Perrin-Terrin A, Jeton F, Pichon A, Frugiere A, Richalet J, Bodineau L, Voituren N (2016) The c-FOS
564 Protein Immunohistological Detection: A Useful Tool As a Marker of Central Pathways Involved
565 in Specific Physiological Responses In Vivo and Ex Vivo. *Jove-Journal of Visualized Experiments*.

566 Peter JC, Tugler J, Eftekhari P, Maurice D, Hoebeke J, Roegel JC (2005) Effects on heart rate of an anti-M2
567 acetylcholine receptor immune response in mice. *FASEB J* 19:943-949.

568 Piomelli D, Astarita G, Rapaka R (2007) A neuroscientist's guide to lipidomics. *Nature reviews* 8:743-754.

569 Pradhan SN, Roth T (1968) Comparative behavioral effects of several anticholinergic agents in rats.
570 *Psychopharmacologia* 12:358-366.

571 Rinaldo L, Hansel C (2013) Muscarinic acetylcholine receptor activation blocks long-term potentiation at
572 cerebellar parallel fiber-Purkinje cell synapses via cannabinoid signaling. *Proceedings of the*
573 *National Academy of Sciences of the United States of America* 110:11181-11186.

574 Rogers R, Hermann G, Travagli R, Johnson L (2006) Brainstem Control of Gastric Function. *Physiology of*
575 *the Gastrointestinal Tract, Vols 1 and 2, 4th Edition:851-875.*

576 Ruiz de Azua I, Gautam D, Guettier JM, Wess J (2011) Novel insights into the function of β -cell M3
577 muscarinic acetylcholine receptors: therapeutic implications. *Trends Endocrinol Metab* 22:74-
578 80.

579 Schindelin J, Arganda-Carreras I, Frise E, Kaynig V, Longair M, Pietzsch T, Preibisch S, Rueden C, Saalfeld
580 S, Schmid B, Tinevez J, White D, Hartenstein V, Eliceiri K, Tomancak P, Cardona A (2012) Fiji: an
581 open-source platform for biological-image analysis. *Nature Methods* 9:676-682.

582 Schubert M, Peura D (2008) Control of gastric acid secretion in health and disease. *Gastroenterology*
583 134:1842-1860.

584 Sclafani A (2018) From appetite setpoint to appetition: 50years of ingestive behavior research. *Physiol*
585 *Behav* 192:210-217.

586 Sohn JW, Harris LE, Berglund ED, Liu T, Vong L, Lowell BB, Balthasar N, Williams KW, Elmquist JK (2013)
587 Melanocortin 4 receptors reciprocally regulate sympathetic and parasympathetic preganglionic
588 neurons. *Cell* 152:612-619.

589 Stella N, Schweitzer P, Piomelli D (1997) A second endogenous cannabinoid that modulates long-term
590 potentiation. *Nature* 388:773-778.

591 Straiker A, Mackie K (2007) Metabotropic suppression of excitation in murine autaptic hippocampal
592 neurons. *The Journal of physiology* 578:773-785.

593 Sykaras AG, Demenis C, Case RM, McLaughlin JT, Smith CP (2012) Duodenal enteroendocrine I-cells
594 contain mRNA transcripts encoding key endocannabinoid and fatty acid receptors. *PLoS ONE*
595 7:e42373.

596 Tao J, Campbell J, Tsai L, Wu C, Liberles S, Lowell B (2021) Highly selective brain-to-gut communication
597 via genetically defined vagus neurons. *Neuron* 109:2106-+.

598 Wiley M, Perez P, Argueta D, Avalos B, Wood C, DiPatrizio N (2021) UPLC-MS/MS Method for Analysis of
599 Endocannabinoid and Related Lipid Metabolism in Mouse Mucosal Tissue. *Frontiers in*
600 *Physiology* 12.

601 Wiley MB, DiPatrizio NV (2022) Diet-Induced Gut Barrier Dysfunction Is Exacerbated in Mice Lacking
602 Cannabinoid 1 Receptors in the Intestinal Epithelium. *Int J Mol Sci* 23.

603 Williams KW, Elmquist JK (2012) From neuroanatomy to behavior: central integration of peripheral
604 signals regulating feeding behavior. *Nature neuroscience* 15:1350-1355.

605 Zhang C, Barkholt P, Nielsen J, Thorbek D, Rigbolt K, Vrang N, Woldbye D, Jelsing J (2020) The
606 dorsomedial hypothalamus and nucleus of the solitary tract as key regulators in a rat model of
607 chronic obesity. *Brain Research* 1727.

608 Zhao Y, Tzounopoulos T (2011) Physiological activation of cholinergic inputs controls associative synaptic
609 plasticity via modulation of endocannabinoid signaling. *J Neurosci* 31:3158-3168.

610

611 **Figure Legends**

612

613 **Figure 1. Increased cFos immunoreactivity in the DMV of DIO mice.** cFos immunoreactivity was
614 quantified in the DMV of mice fed, **A**, standard diet (SD) and mice fed, **B**, western diet (WD) 45-75
615 minutes following the onset of the dark period. **C**, The number of cFos⁺ cells was significantly increased

616 in WD mice when compared to SD mice ($t_{(10)} = 5.575$; $p = 0.0002$; unpaired Student's t test). **D**, cFos
617 immunoreactivity (panel 1), ChAT immunoreactivity (panel 2), and merged (panel 3) images of the DMV
618 in SD mice (top row) and WD mice (bottom row). **E**, The number of cFos⁺ cells was significantly increased
619 in the second cohort of WD mice compared to SD controls ($t_{(10)} = 2.462$; $p = 0.0335$; unpaired Student's t
620 test). **F**, The number of cells co-labeled with both cFos and ChAT was significantly increased in the DMV
621 of WD-fed mice ($t_{(10)} = 2.342$; $p = 0.0412$; unpaired Student's t test). **G**, 73.33% of cFos⁺ cells in WD-fed
622 animals were also immunoreactive for ChAT, while 57.93% of cFos⁺ cells in SD-fed animals were
623 immunoreactive for ChAT. There was no significant difference in the ratio of ChAT⁺/cFos⁺ cells between
624 WD- and SD-fed groups. All data are presented as mean \pm SEM, $n = 6$ mice per diet, *** $p < 0.001$. AP =
625 Area Postrema, CC = Central Canal, 4V = Fourth Ventricle.

626

627 **Figure 2. Mice fed western diet (WD) become obese and hyperphagic.** **A**, Body weight was recorded bi-
628 weekly between 0900h and 1000h (time x diet interaction: $F_{(16,480)} = 121.8$; $p < 0.0001$; diet main effect
629 $F_{(1,30)} = 79.56$; $p < 0.0001$; 2-way ANOVA followed by Holm Sidak's multiple comparisons test). **B**, Change
630 in body mass (time x diet interaction: $F_{(16,480)} = 121.8$; $p < 0.0001$; diet main effect $F_{(1,30)} = 195.4$; $p <$
631 0.0001 ; 2-way ANOVA followed by Holm Sidak's multiple comparisons test). **C**, Total caloric intake
632 during a 24 h test period ($t_{(30)} = 3.666$; $p = 0.0009$; unpaired Student's t test). **D**, At the end of the 60-day
633 diet exposure period to western diet (WD), epididymal fat pads were weighed ($t_{(30)} = 9.686$; $p > 0.0001$;
634 unpaired Student's t test). All data are presented as mean \pm SEM, $n = 16$ per diet; * $p < 0.05$, ** $p < 0.01$,
635 *** $p < 0.001$, **** $p < 0.0001$.

636

637 **Figure 3. mAChR antagonists block MAG formation in the jejunum epithelium of DIO mice.** Mice fed
638 standard diet (SD) or western diet (WD) were treated with a single IP injection of vehicle, DAU5884 (2

639 mg/kg) or PIR (2 mg/kg) 30 minutes prior to tissue harvest (cohort 1). A second group (cohort 2) of WD
640 mice was treated with vehicle or ATR (2 mg/kg), and otherwise processed identically to cohort 1. **A**, 2-
641 AG and other MAGs in upper small-intestinal epithelium tissue were isolated via lipid extraction and
642 quantitated using UPLC-MS/MS. 2-AG was significantly elevated in vehicle-treated WD mice when
643 compared to vehicle-treated SD mice. Treatment with DAU or ATR in WD mice restored levels of 2-AG to
644 levels in SD control mice (cohort 1: $F_{(3,28)} = 3.721$, $P = 0.0227$; SD vehicle vs. WD vehicle $p = 0.0448$; WD
645 vehicle vs WD DAU $p = 0.0402$; 1-way ANOVA followed by Holm Sidak's multiple comparisons test;
646 cohort 2: $t_{(18)} = 2.510$; $p = 0.0218$; unpaired Student's t test). **B**, 2-DG was significantly elevated in
647 vehicle-treated WD mice compared to vehicle-treated SD mice. Treatment with DAU or ATR in WD mice
648 restored levels of 2-AG to that of SD mice (cohort 1: $F_{(3,28)} = 4.691$, $P = 0.0089$; SD vehicle vs. WD vehicle
649 $p = 0.0200$; WD vehicle vs WD DAU $p = 0.0159$; 1-way ANOVA followed by Holm Sidak's multiple
650 comparisons test; cohort 2: $t_{(18)} = 2.115$; $p = 0.0486$; unpaired Student's t test). **C**, 2-OG was significantly
651 elevated in vehicle-treated WD mice when compared to vehicle-treated SD mice. Treatment with DAU
652 or PIR restored levels of 2-AG in WD mice to those in SD mice (cohort 1: $F_{(3,25)} = 6.657$, $P = 0.0019$; SD
653 vehicle vs. WD vehicle $p = 0.0014$; WD vehicle vs WD DAU $p = 0.0439$; WD vehicle vs WD PIR $p = 0.0315$;
654 1-way ANOVA followed by Holm Sidak's multiple comparisons test; cohort 2: $t_{(17)} = 1.565$; $p = 0.1361$;
655 unpaired Student's t test). **D**, 2-LG levels were not significantly different between any treatment or diet
656 groups (cohort 1: $F_{(3,25)} = 3.346$, $P = 0.0351$; SD vehicle vs. WD vehicle $p = 0.0014$; WD vehicle vs WD DAU
657 $p = 0.0439$; WD vehicle vs WD PIR $p = 0.0315$; 1-way ANOVA followed by Holm Sidak's multiple
658 comparisons test; cohort 2: $t_{(18)} = 1.720$; $p = 0.1026$; unpaired Student's t test). All data are presented as
659 mean \pm SEM, $n = 8-10$ per group; * $p < 0.05$, ** $p < 0.01$.

660

661 **Figure 4. Pirenzepine dose response analysis.** Doses of PIR within one log step of the original 2 mg per
662 kg dose were tested for their ability to inhibit MAG formation in the upper intestinal epithelium and

663 attenuate food intake in WD-fed animals. **A**, 2.0 mg per kg of PIR significantly reduced 2-AG levels
664 compared to the vehicle and 0.65 mg per kg dose ($F_{(3,12)} = 0.310$, $P = 0.0150$; 0.0 vs. 2.0 $p = 0.0265$; 0.65
665 vs 2.0 $p = 0.0265$). **B**, 2.0 mg per kg of PIR significantly reduced 2-DG levels compared to the vehicle and
666 0.65 mg per kg dose ($F_{(3,12)} = 0.8774$, $P = 0.0124$; 0.0 vs. 2.0 $p = 0.0227$; 0.65 vs 2.0 $p = 0.0212$). **C**, PIR did
667 not affect 2-OG levels at any dose ($F_{(3,12)} = 0.635$, $P = 0.1046$). **D**, PIR did not affect 2-LG levels at any dose
668 ($F_{(3,12)} = 0.126$, $P = 0.0847$). **E**, There was a main effect of time and PIR dose on food intake, but no
669 significant differences were detected in the multiple comparisons test (time main effect $F_{(3, 224)} = 43.44$; p
670 < 0.0001 , dose main effect $F_{(3, 224)} = 3.516$; $p = 0.02$). **F**, There was a main effect of time, but not dose, on
671 water intake, but no significant differences were detected in the multiple comparisons test (time main
672 effect $F_{(3, 224)} = 42.31$; $p < 0.001$). **G**, There was a main effect of time, but not dose, on ambulation, but no
673 significant differences were detected in the multiple comparisons test (time main effect $F_{(3, 224)} = 32.23$; p
674 < 0.0001). **A-D** are 1-way ANOVAs followed by Holm-Sidak's multiple comparisons test when
675 appropriate, $n = 4$ per dose, **E-G** are 2-way ANOVAs followed by Holm-Sidak's multiple comparisons test
676 when appropriate, $n = 15$. All data are presented as mean \pm SEM; * $p < 0.05$.

677

678 **Figure 5. SAG formation and DGL Activity in upper intestinal epithelium are inhibited by mAChR**
679 **antagonism in DIO mice.** Levels of SAG in the upper small-intestinal epithelium tissue were isolated and
680 quantitated using UPLC-MS/MS. The same tissue was analyzed for DGL and MGL activity using an
681 enzymatic assay; enzyme reaction products were isolated and quantitated via UPLC-MS/MS. Enzyme
682 activity was calculated using the nmols of reaction product generated per mg of tissue per minute of the
683 reaction. **A**, SAG was significantly elevated in vehicle-treated mice fed western diet (WD) compared to
684 vehicle-treated mice fed standard diet (SD). Treatment with DAU, PIR, or ATR in WD mice restored levels
685 of SAG to that of lean controls (cohort 1: $F_{(3,27)} = 14.76$, $P < 0.0001$; SD Veh vs. WD Veh $p = 0.0004$; WD
686 Veh vs WD DAU $p < 0.0001$; WD Veh vs WD PIR $p < 0.0001$; 1-way ANOVA followed by Holm Sidak's

687 multiple comparisons test; cohort 2: $t_{(18)} = 5.010$; $p = 0 < 0.0001$; unpaired Student's t test). **B**, DGL activity
688 was significantly elevated in vehicle-treated WD mice compared to vehicle-treated SD mice. Treatment
689 with DAU, PIR, or ATR in WD mice restored DGL activity to that of lean controls (cohort 1: $F_{(3,26)} = 10.57$,
690 $P = 0.0001$; SD Veh vs. WD Veh $p = 0.0030$; WD Veh vs WD DAU $p = 0.0013$; WD Veh vs WD PIR $p =$
691 0.0001 ; 1-way ANOVA followed by Holm Sidak's multiple comparisons test; cohort 2: $t_{(17)} = 2.546$; $p =$
692 0.0209 ; unpaired Student's t test). **C**, MGL activity was not different between any diet or treatment
693 group (cohort 1: $F_{(3,27)} = 2.537$, $P = 0.0777$; 1-way ANOVA; cohort 2: $t_{(18)} = 2.081$; $p = 0.0520$; unpaired
694 Student's t test). All data are presented as mean \pm SEM, $n = 8-10$ per group; * $p < 0.05$, ** $p < 0.01$, *** $p <$
695 0.001 , **** $p < 0.0001$. **D**, Schematic illustrating that activation of G_q -coupled mAChRs initiates the PLC-
696 dependent generation of SAG, which is subsequently converted to 2-AG by DGL. 2-AG is further
697 hydrolyzed by MGL into glycerol and arachidonic acid. Illustration created with BioRender.com

698

699 **Figure 6. Anticholinergics do not affect 2-AG metabolic enzyme activity *ex vivo*.** Activity of DGL in the
700 upper small-intestinal epithelium from mice fed western diet (WD) was assayed in the presence
701 increasing concentrations of a DGL-specific inhibitor and various mAChR antagonists. **A**, DGL activity was
702 inhibited in a concentration-dependent manner when incubated with THL at concentrations ranging
703 from 3-1,000 nM ($IC_{50} = 58.52$ nM, $R^2 = 0.9499$). **B**, DGL activity was not directly inhibited by ATR at
704 concentrations ranging from 10-10,000 nM ($R^2 = -0.0212$). **C**, DGL activity was not directly inhibited by
705 DAU at concentrations ranging from 10-10,000 nM ($R^2 = -0.0286$). **D**, DGL activity was not directly
706 inhibited by PIR at concentrations ranging from 10-10,000 nM ($R^2 = -0.0113$). All data are presented as
707 mean \pm SEM, $n = 3$ animals per drug. All graphs are least squares fit of $\log[\text{inhibitor}]$ vs. normalized
708 response.

709

710 **Figure 7. Anticholinergics inhibit food intake in DIO mice. A,** AM6545 (10 mg/kg), ATR (2 mg/kg), or a
711 combination of AM6545 + ATR reduced caloric intake for up to 24 hours in western diet-fed (WD) mice
712 (time x drug interaction: $F_{(9,158)} = 4.639$; $p < 0.0001$; drug main effect $F_{(3,54)} = 4.560$; $p = 0.0064$; 12 hour
713 vehicle vs. 12 hour ATR $p = 0.0175$, 12 hour vehicle vs. 12 hour AM6545 $p = 0.0143$, 12 hour vehicle vs.
714 12 hour combination $p = 0.0020$, 24 hour vehicle vs. 24 hour ATR $p = 0.0301$, 24 hour vehicle vs. 24 hour
715 AM6545 $p = 0.0145$, 24 hour vehicle vs. 24 hour combination $p = 0.0049$; 2-way ANOVA followed by
716 Holm Sidak's multiple comparisons test). **B,** AM6545, ATR, or both drugs in combination did not affect
717 caloric intake in standard diet-fed (SD) mice (time x drug interaction: $F_{(9,164)} = 0.9117$; $p = 0.5165$; time
718 main effect $F_{(2,103,115.0)} = 142.4$; $p < 0.0001$; drug main effect $F_{(3,56)} = 1.69$; $p = 0.1799$; 2-way ANOVA). **C,**
719 DAU5884 (2 mg/kg) reduced caloric intake for up to 12 hours in WD mice (time x drug interaction: $F_{(3,84)}$
720 $= 1.239$; $p = 0.3009$; drug main effect $F_{(1,28)} = 6.750$; $p = 0.0148$; 1 hour vehicle vs. 1 hour DAU $p = 0.0358$,
721 6 hour vehicle vs. 6 hour DAU $p = 0.0168$, 12 hour vehicle vs. 12 hour DAU $p = 0.0358$; 2-way ANOVA
722 followed by Holm Sidak's multiple comparisons test). **D,** DAU5884 did not affect caloric intake in SD mice
723 for 24 hours (time x drug interaction: $F_{(3,70)} = 0.5839$; $p = 0.6276$; drug main effect $F_{(1,24)} = 0.2090$; $p =$
724 0.6517 ; 2-way ANOVA). **E,** PIR (2 mg/kg) did not affect caloric intake in WD mice (time x drug interaction:
725 $F_{(3,80)} = 1.526$; $p = 0.2140$; drug main effect $F_{(1,28)} = 0.1463$; $p = 0.7050$; 2-way ANOVA). **F,** PIR did not
726 affect caloric intake in standard diet-fed mice (time x drug interaction: $F_{(3,79)} = 1.781$; $p = 0.1576$; drug
727 main effect $F_{(1,28)} = 0.07073$; $p = 0.7922$; 2-way ANOVA). All data are presented as mean \pm SEM, $n = 15 -$
728 16 ; * $p < 0.05$, ** $p < 0.01$.

729

730 **Figure 8. Effects of drug treatments on ambulation and water intake.** Total distance travelled and
731 cumulative water intake was measured by automated feeding chambers for a 24-hour period starting at
732 the onset of the dark cycle (1800h) following a single IP injection of AM6545 (10 mg/kg), ATR (2 mg/kg),

733 DAU (2 mg/kg), and PIR (2 mg/kg). **A**, ATR and AM6545 alone or in combination reduced distance
734 travelled for up to 12 h in mice fed western diet (WD). **C**, AM6545 resulted in decreased cumulative
735 distance travelled at the 12 h timepoint in mice fed standard diet (SD). AM6545 and ATR combined
736 reduced ambulation across the 24 h test. **B & D**, AM6545 and ATR alone combined had no significant
737 effects on water intake across the 24 h test in mice fed SD or WD. **E & F**, A single IP injection of DAU
738 yielded no significant effects on distance travelled in mice fed SD or WD. **G**, DAU did not significantly
739 affect water intake for the 24 h test in mice fed SD. **H**, In mice fed WD and treated with DAU, water
740 intake was affected by drug alone, as well as a time x drug interaction, although there were no
741 significant differences at individual time points as revealed by the Holm-Sidak multiple comparisons test.
742 **I & J**, A single IP injection of PIR yielded no significant effects on distance travelled in mice fed SD or WD
743 for the 24 h test. **K & L**, Treatment with PIR also had no effect on water intake in mice fed with SD or WD
744 for the 24 h test. 2-Way ANOVA followed by Holm-Sidak's multiple comparisons test when appropriate,
745 see **Table 1** for detailed statistics. All data are presented as mean \pm SEM, $n = 15 - 16$; * $p < 0.05$, ** $p <$
746 0.01 , *** $p < 0.001$, **** $p < 0.0001$.

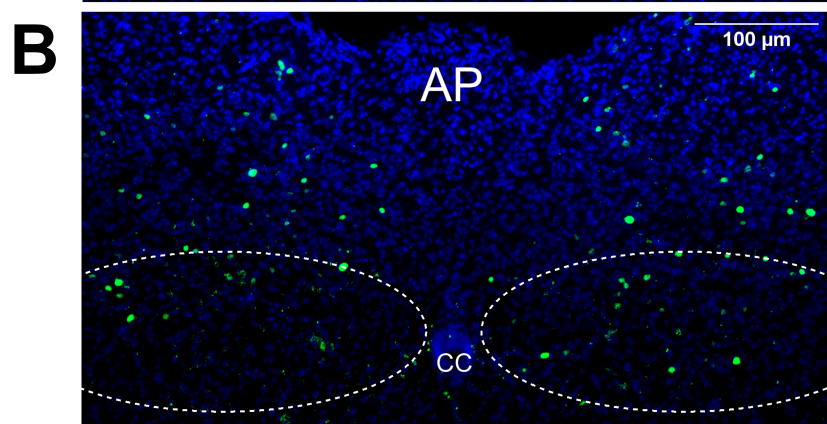
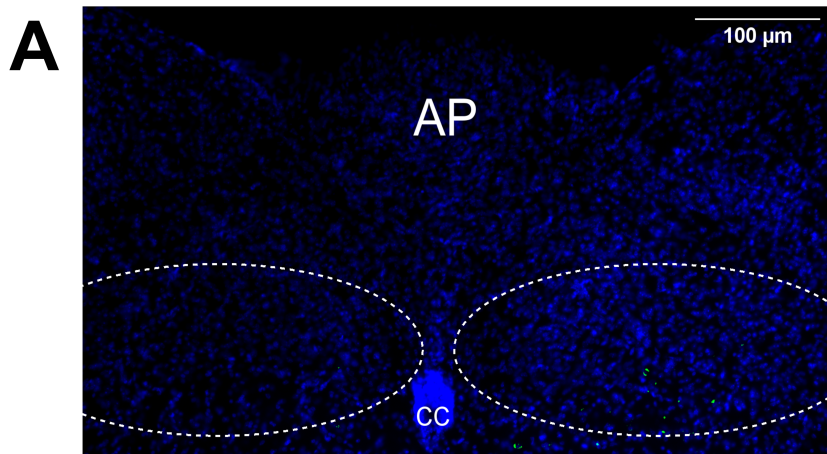
747

748 **Figure 9. Inhibiting peripheral CB₁Rs or mAChRs failed to affect food intake in mice conditionally**
749 **lacking CB₁Rs in the intestinal epithelium.** **A**, AM6545 (10 mg/kg) or ATR (2 mg/kg) reduced caloric
750 intake for up to 24 hours in control intCB₁^{+/+} mice (time x drug interaction: $F_{(6,79)} = 5.099$; $p = 0.0002$;
751 drug main effect $F_{(2,30)} = 6.024$; $p = 0.0063$; 12 hour vehicle vs. 12 hour AM6545 $p = 0.0498$, 24 hour
752 vehicle vs. 24 hour AM6545 $p = 0.0012$, 24 hour vehicle vs. 24 hour ATR $p = 0.0043$, 2-way ANOVA
753 followed by Holm Sidak's multiple comparisons test). **B**, AM6545 or ATR did not affect caloric intake in
754 intCB₁^{-/-} mice (time x drug interaction: $F_{(6,135)} = 0.7700$; $p = 0.5948$; drug main effect $F_{(2,45)} = 0.9273$; $p =$
755 0.4030 ; 2-way ANOVA). **C**, Body weights were similar between intCB₁^{-/-} when compared to intCB₁^{+/+}
756 mice control mice fed western diet (WD; time x genotype interaction: $F_{(9,225)} = 5.327$; $p < 0.0001$;

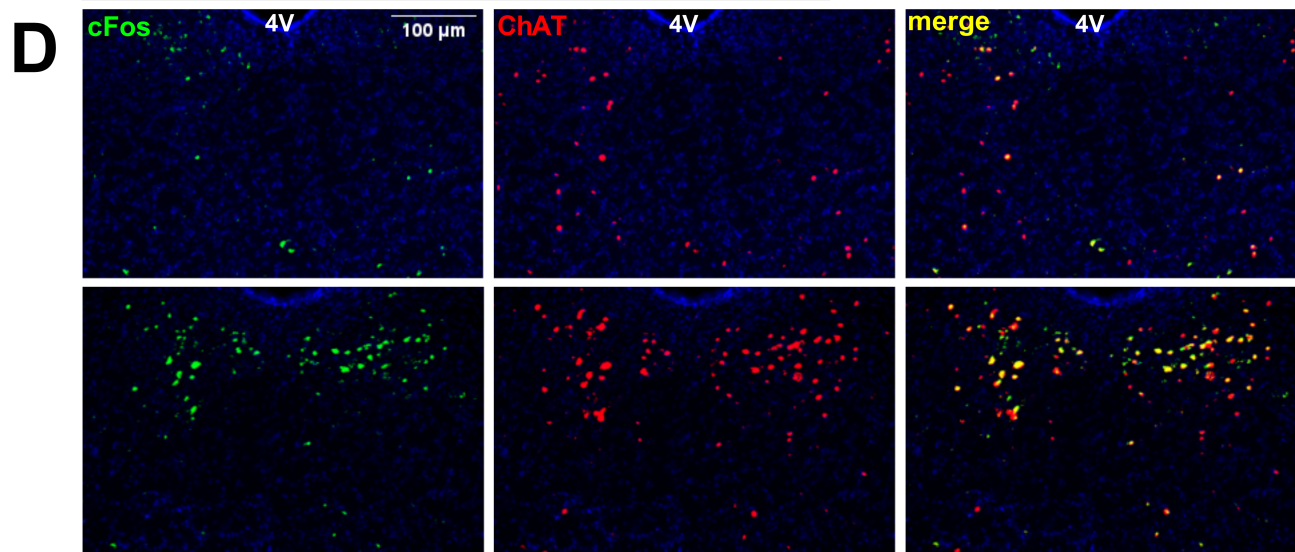
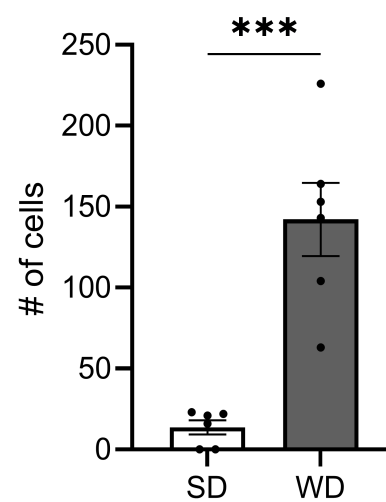
757 genotype main effect $F_{(1,25)} = 0.01602$; $p = 0.9003$; 2-way ANOVA followed by Holm Sidak's multiple
758 comparisons test). **D**, Change in body weight was lower in intCB₁^{-/-} when compared to intCB₁^{+/+} control
759 mice (time x genotype interaction: $F_{(9,225)} = 5.327$; $p < 0.0001$; genotype main effect $F_{(1,25)} = 5.077$; $p =$
760 0.0333 ; 2-way ANOVA followed by Holm Sidak's multiple comparisons test). All data are presented as
761 mean \pm SEM, n = 16, 11 (intCB₁^{-/-}, intCB₁^{+/+} respectively), $p < 0.05$, $**p < 0.01$.

762

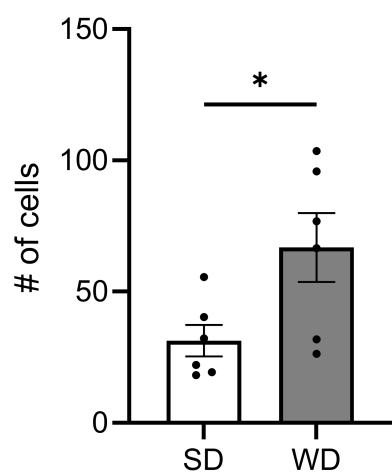
763 **Figure 10. Effects of drug treatments on ambulation and water intake in mice with conditional**
764 **deletion of CB₁Rs in the intestinal epithelium fed western diet (WD). A-B**, Total distance travelled and,
765 **C-D**, cumulative water intake was measured by automated feeding chambers for a 24-hour period
766 starting at the onset of the dark cycle (1800h) following a single IP injection of AM6545 (10 mg/kg) or
767 ATR (2 mg/kg) in intCB₁^{+/+} and intCB₁^{-/-} fed WD. **A**, A single dose of AM6545 in IntCB₁^{+/+} controls
768 affected distance travelled across the entire 24-hour testing period. ATR also reduced distance travelled
769 in the same mice at the 1- and 24-hour timepoints. **B**, There was a significant effect of drug and drug x
770 time interaction in IntCB₁^{-/-} mice on distance travelled, but the Holm-Sidak multiple comparisons *post*
771 *hoc* analysis did not reveal any significant differences at individual time points. **C**, Water intake of
772 intCB₁^{+/+} mice was not significantly affected by either drug treatment for the 24 h test. **D**, There was a
773 significant effect of drug, as well as a drug x time interaction on water intake in intCB₁^{-/-} animals.
774 Specifically, AM6545 treatment significantly reduced cumulative water intake at the 1-, 6-, and 24-h
775 timepoints. 2-way ANOVA followed by Holm-Sidak's multiple comparisons test when appropriate, see
776 **Table 2** for detailed statistics. All data are presented as mean \pm SEM, n = 11 or 16 (intCB₁^{+/+} and intCB₁^{-/-}
777 ^{-/-}, respectively); * $p < 0.05$, ** $p < 0.01$, *** $p < 0.001$, **** $p < 0.0001$.



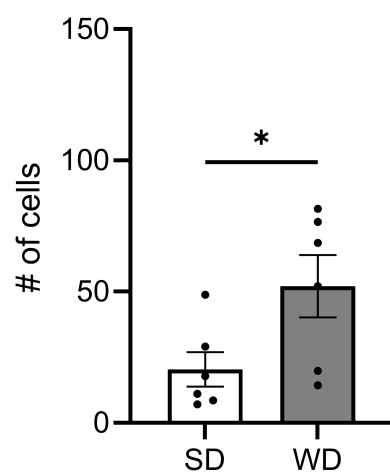
C cFos⁺ cells in DMV



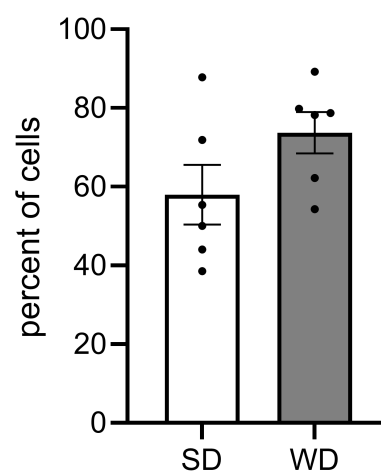
E cFos⁺ cells

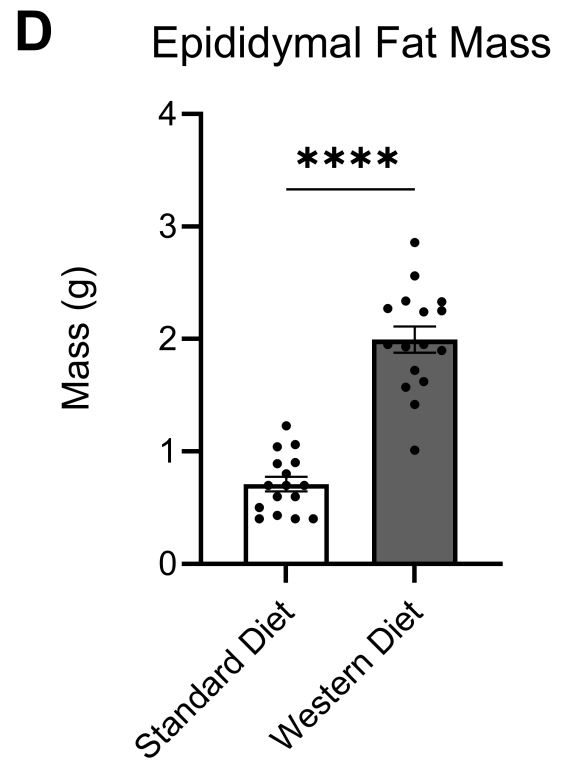
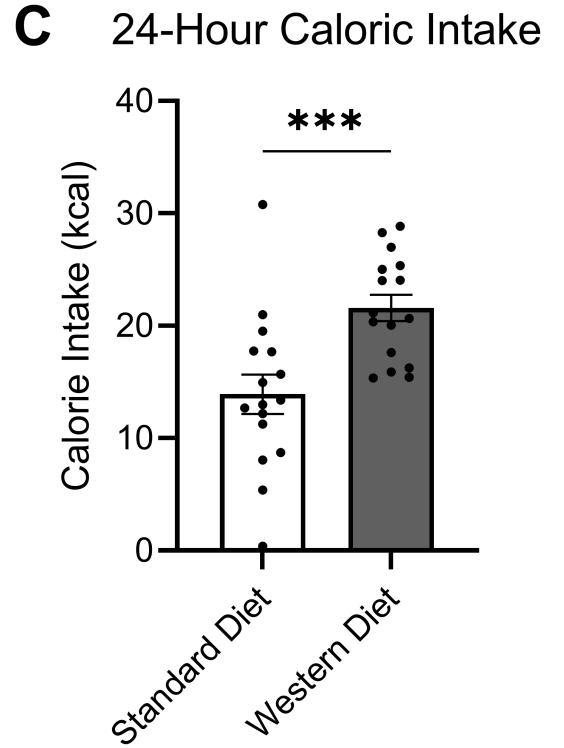
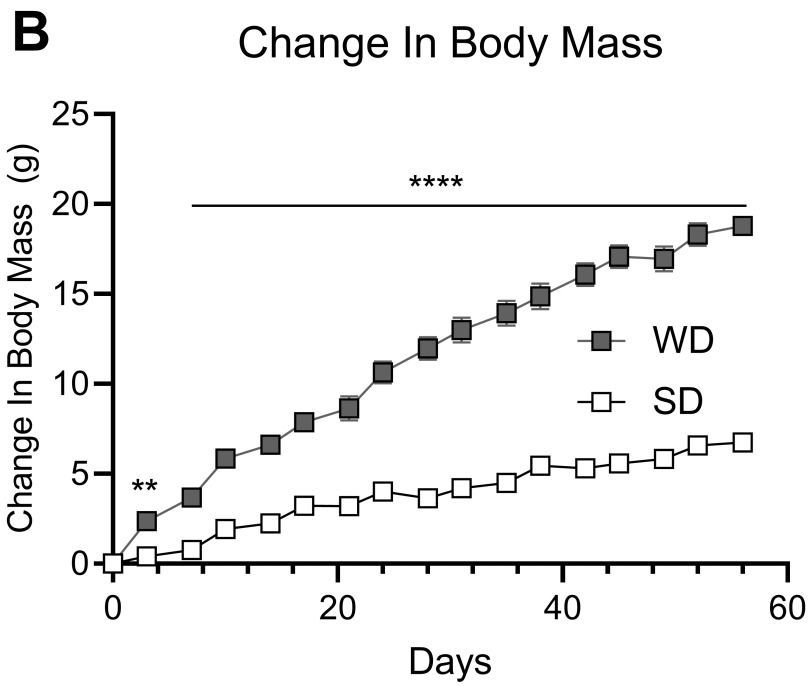
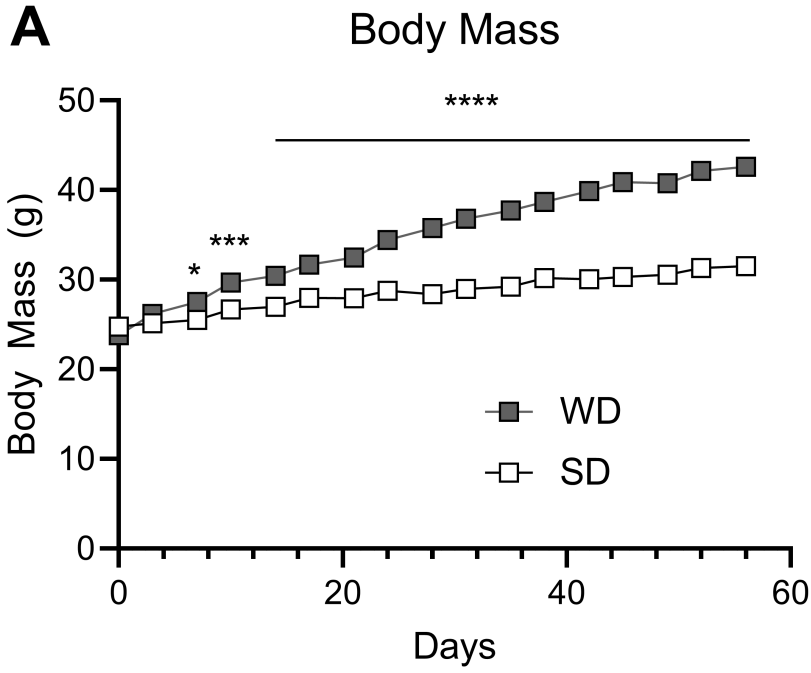


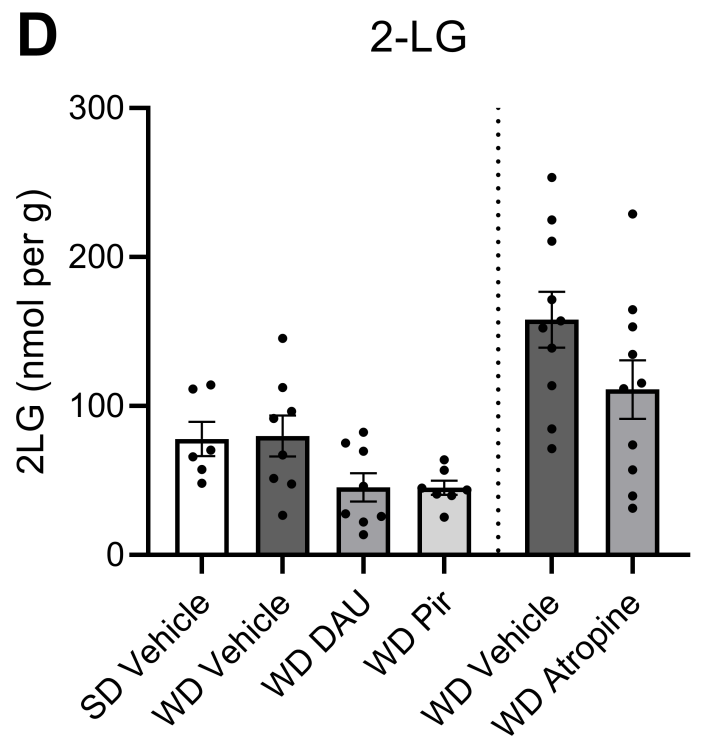
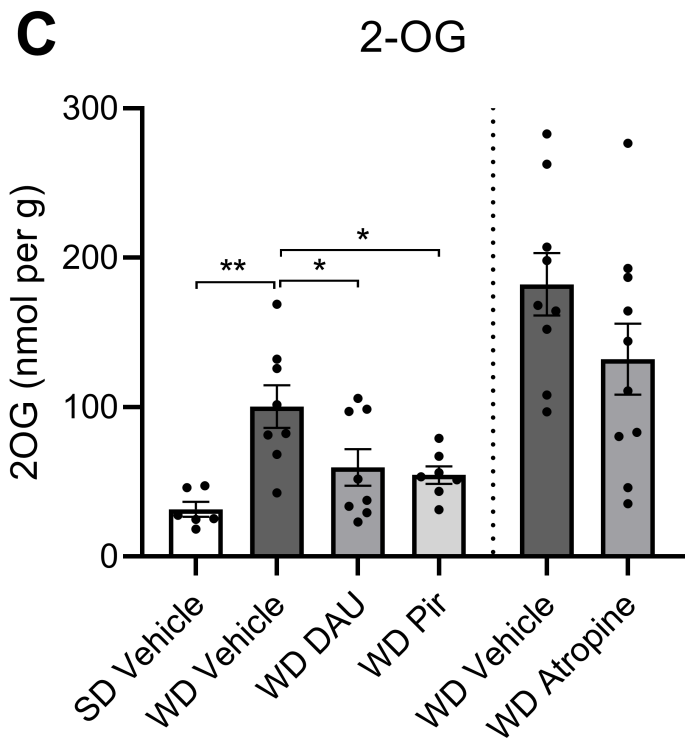
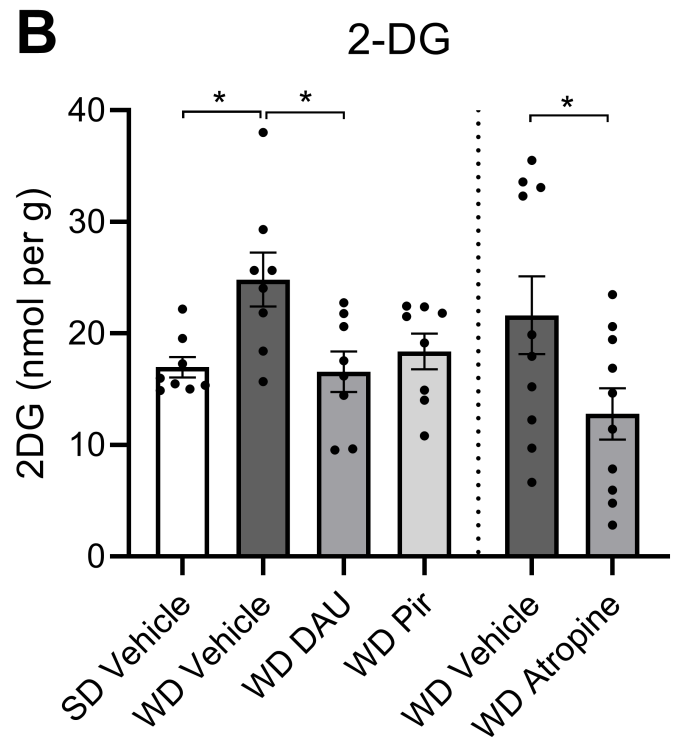
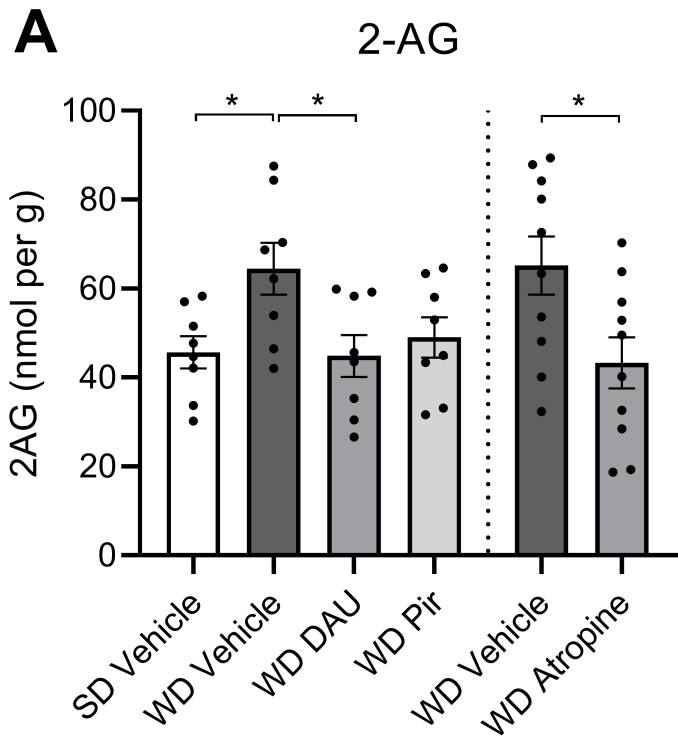
F Dual-labeled cells

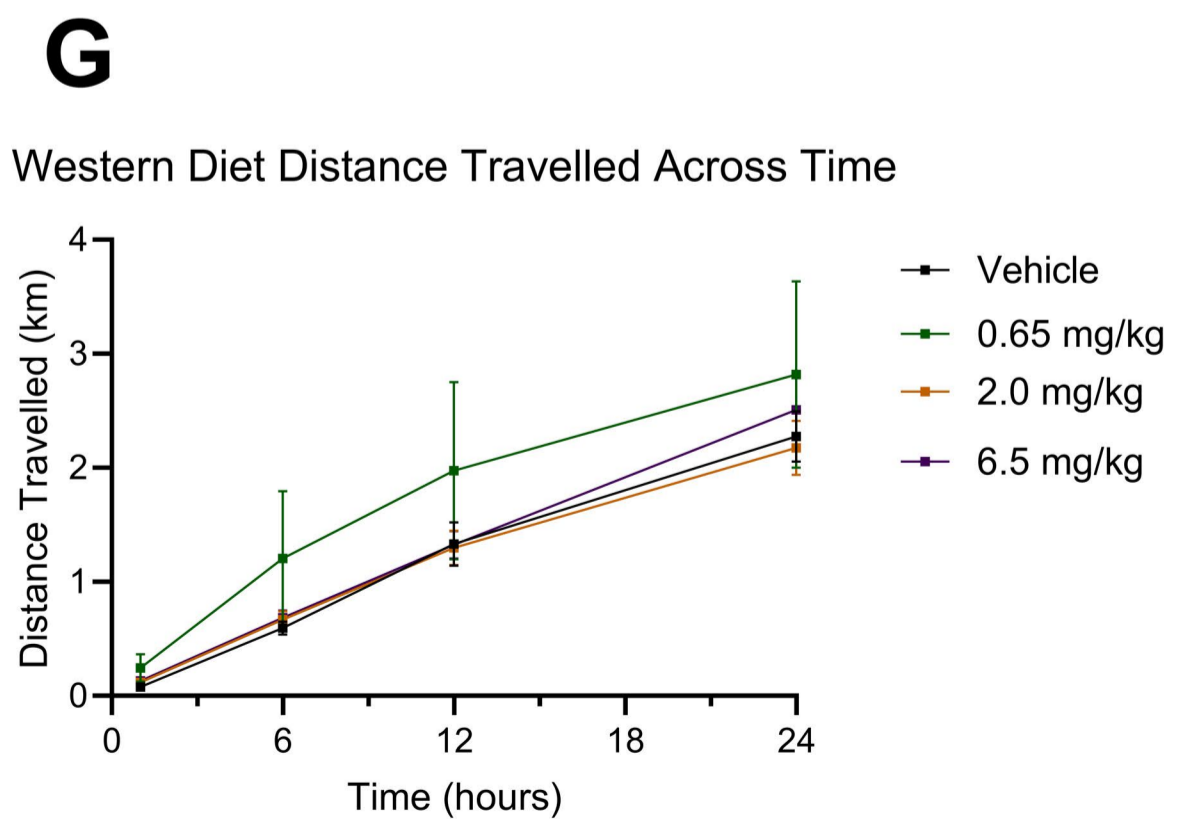
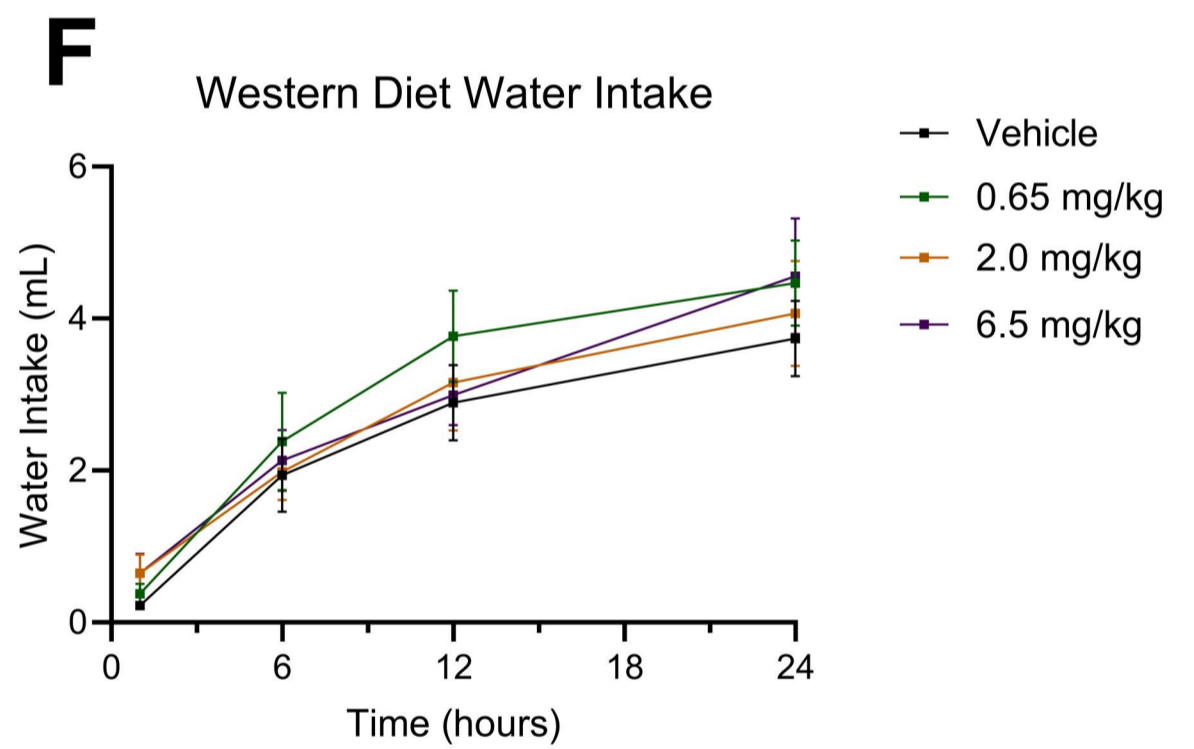
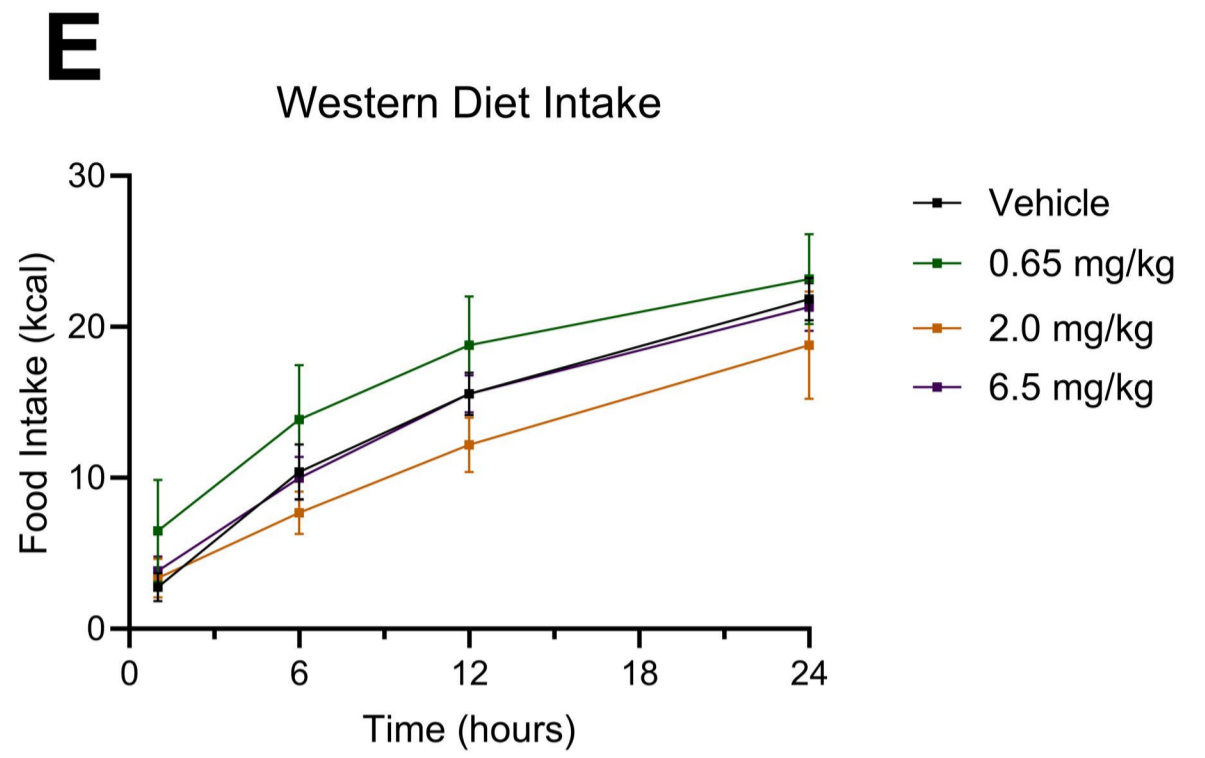
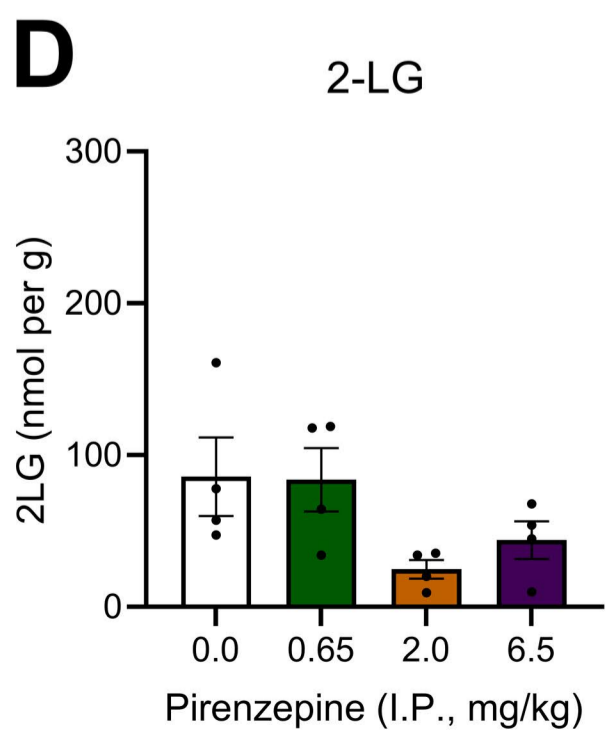
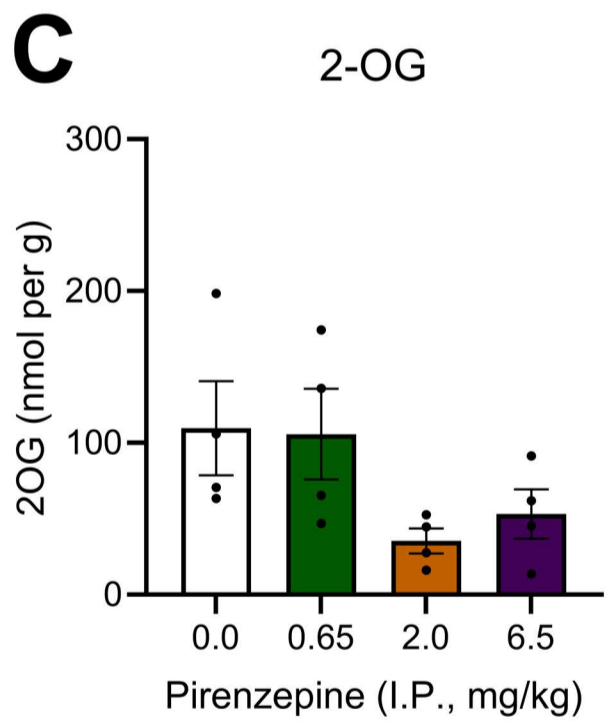
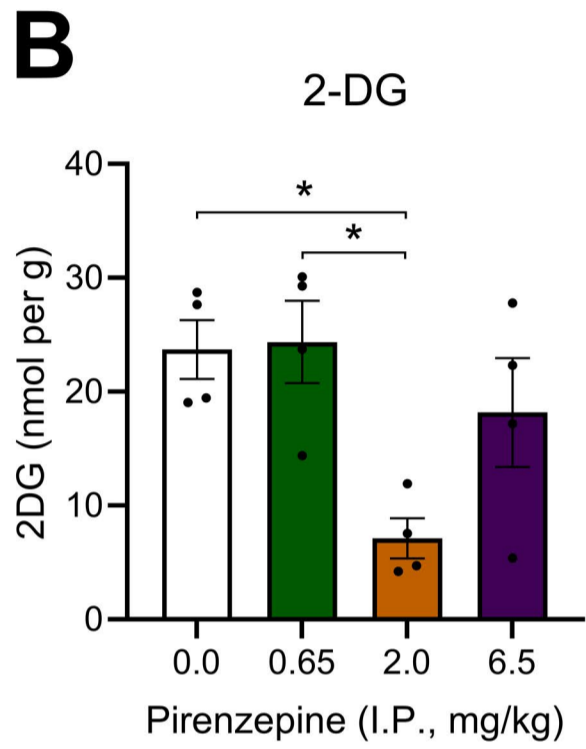
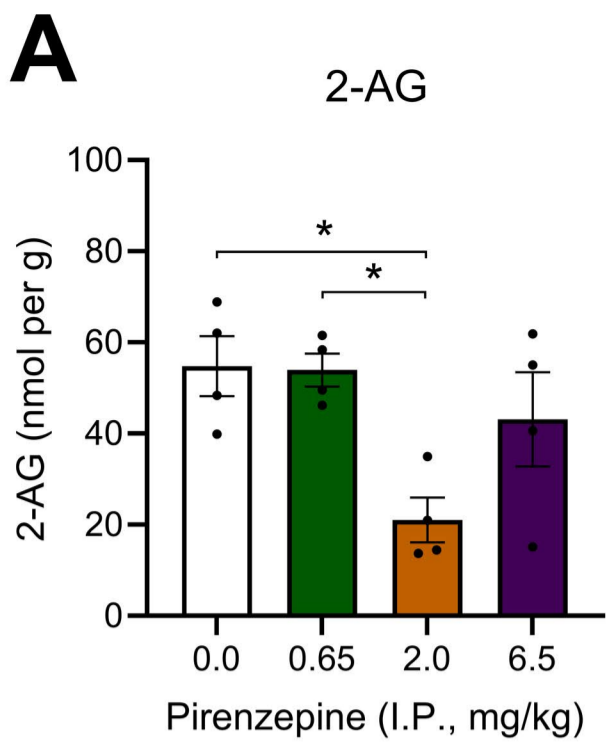


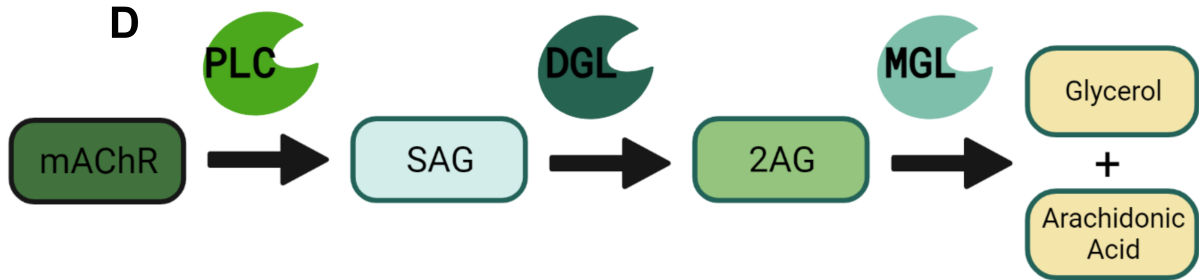
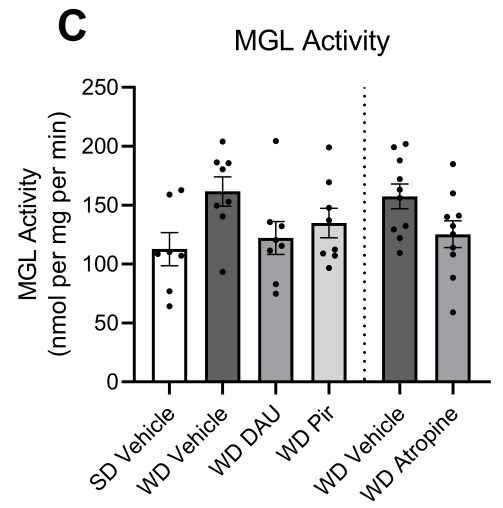
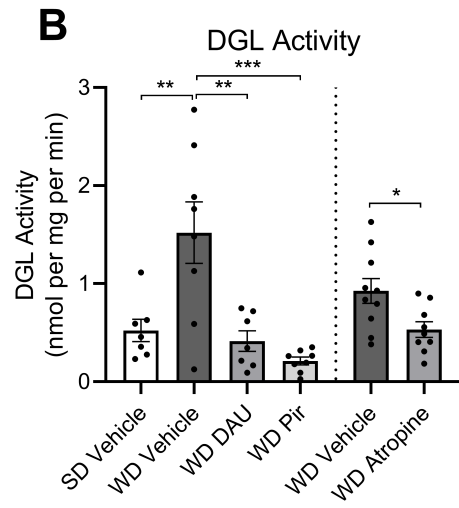
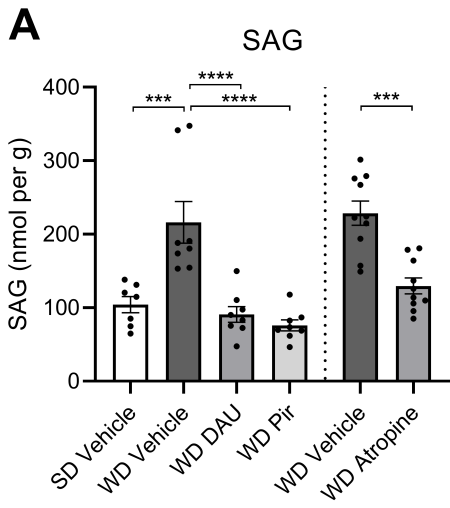
G ChAT⁺/cFos⁺ Cells



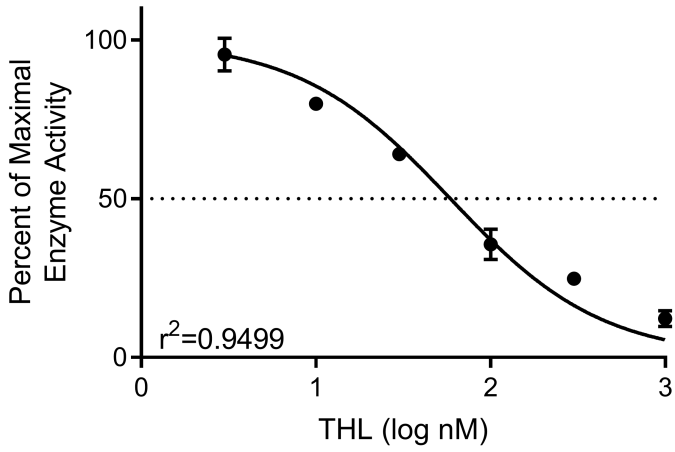




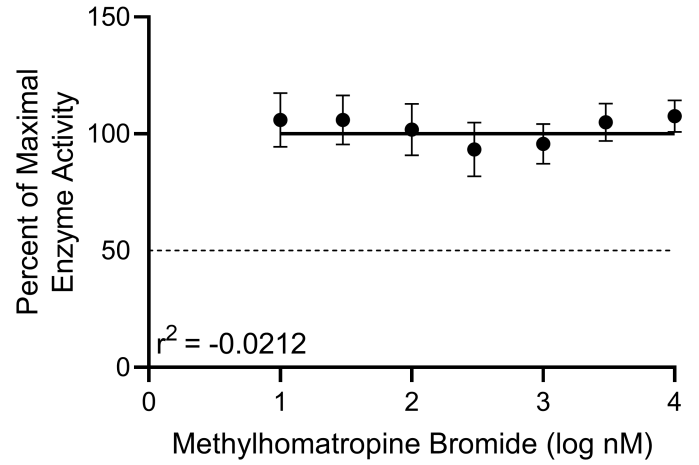




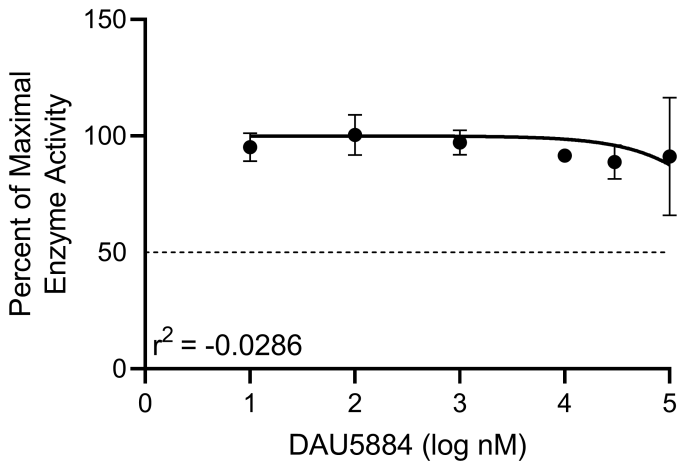
A Jejunum Mucosa DGL Inhibition



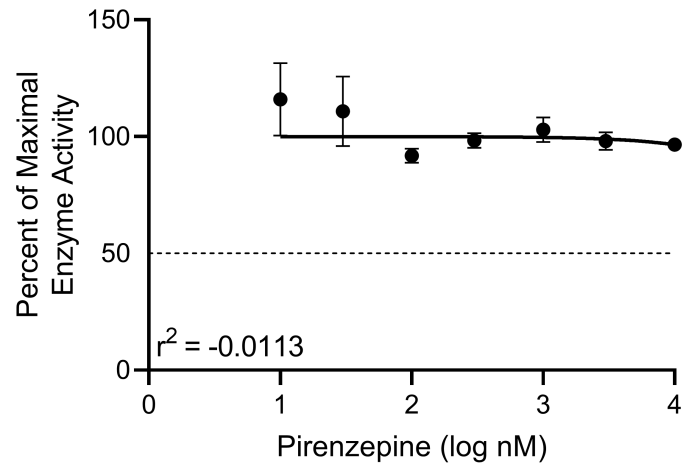
B Jejunum Mucosa DGL Activity

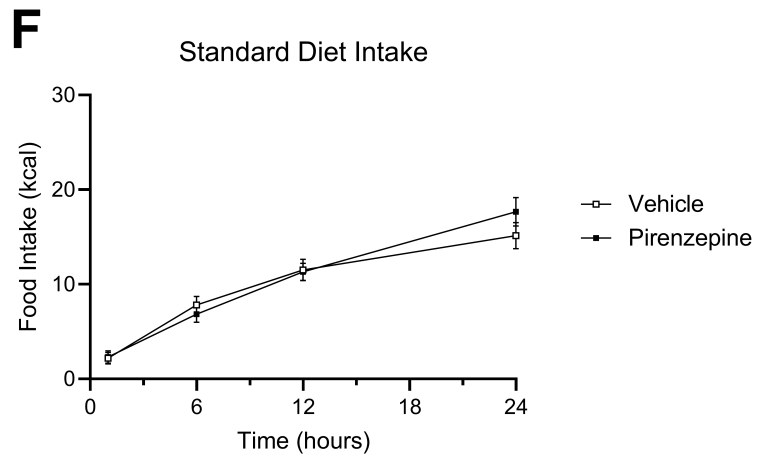
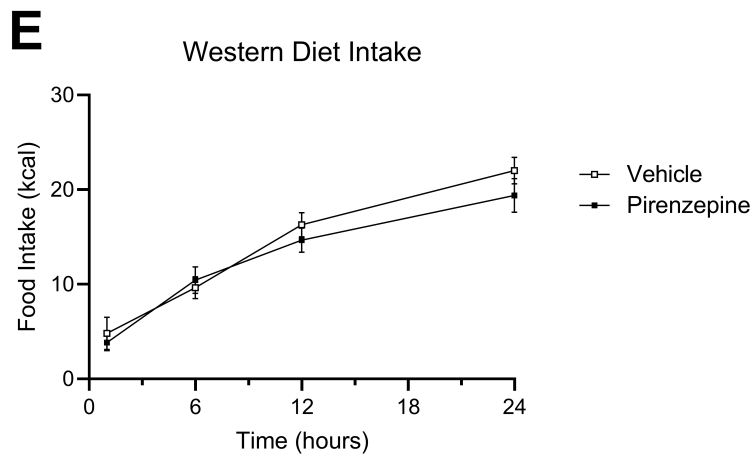
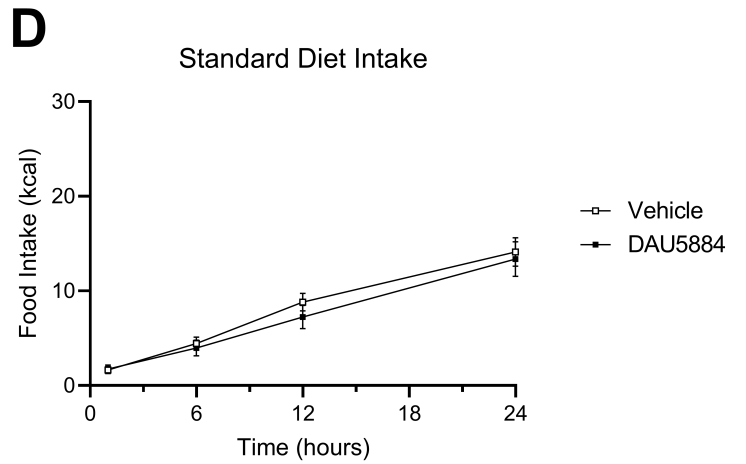
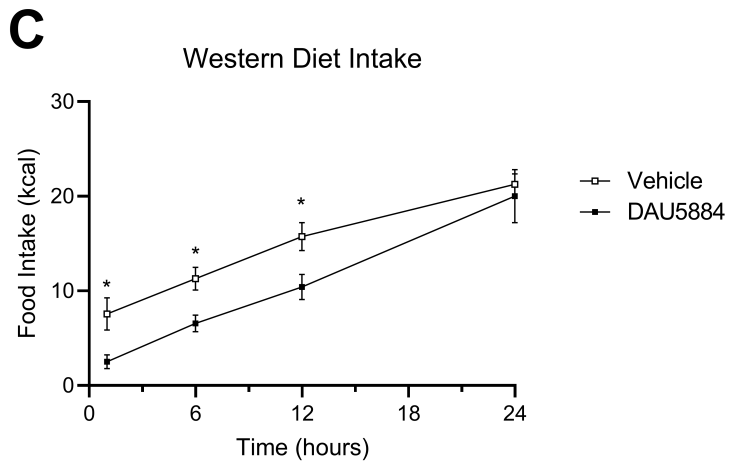
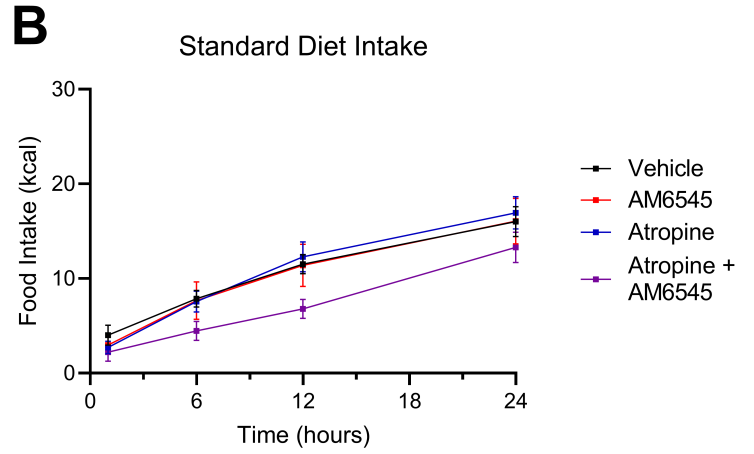
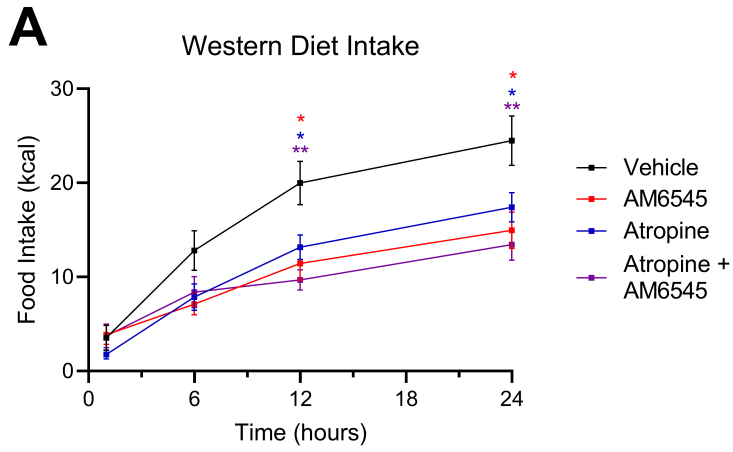


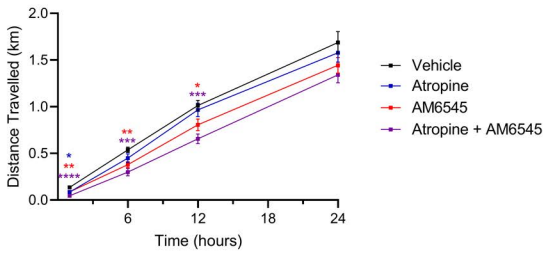
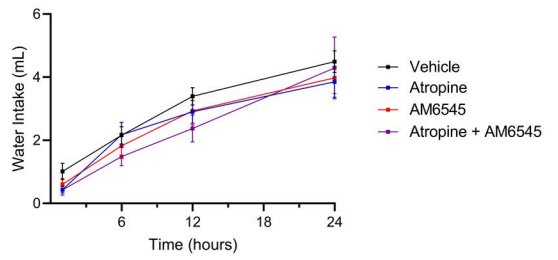
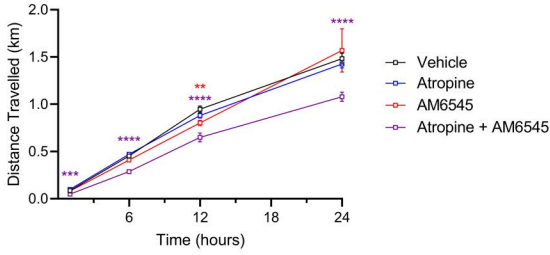
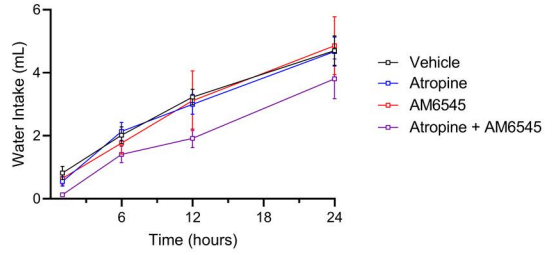
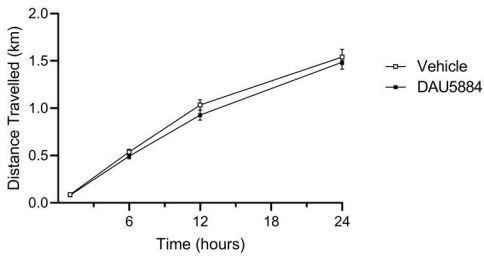
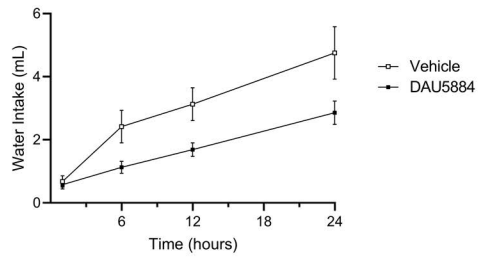
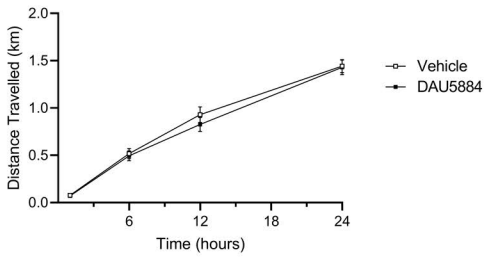
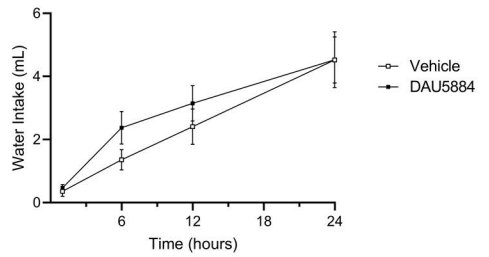
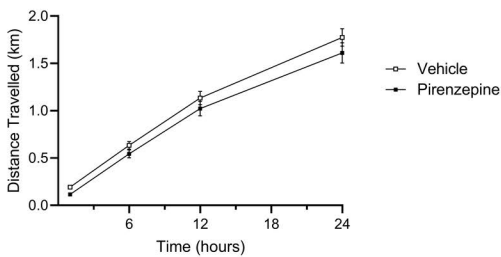
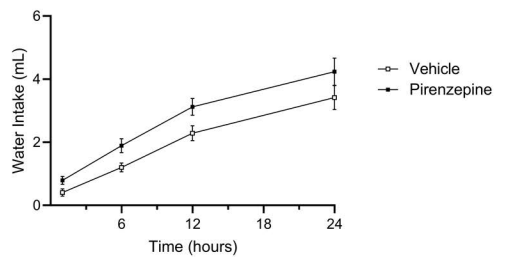
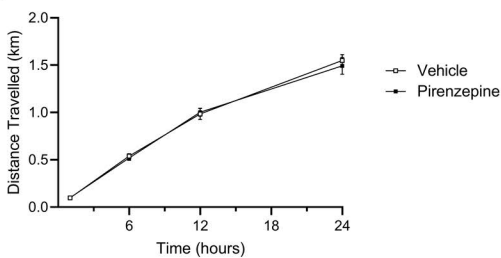
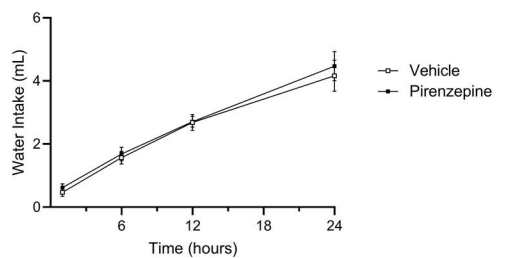
C Jejunum Mucosa DGL Activity



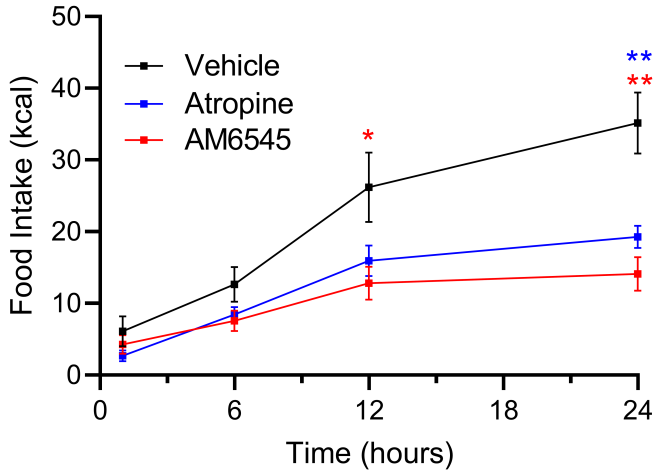
D Jejunum Mucosa DGL Activity



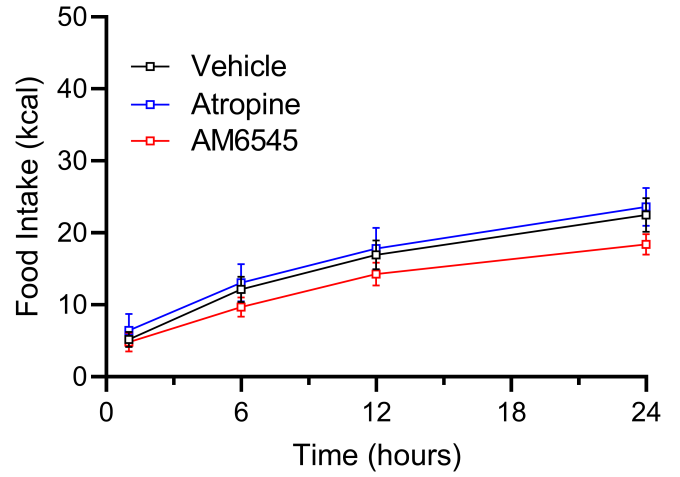


A Western Diet Distance Travelled Across Time**B** Western Diet Water Intake Across Time**C** Standard Diet Distance Travelled Across Time**D** Standard Diet Water Intake Across Time**E** Western Diet Distance Travelled Across Time**F** Western Diet Water Intake Across Time**G** Standard Diet Distance Travelled Across Time**H** Standard Diet Water Intake Across Time**I** Western Diet Distance Travelled Across Time**J** Western Diet Water Intake Across Time**K** Standard Diet Distance Travelled Across Time**L** Standard Diet Water Intake Across Time

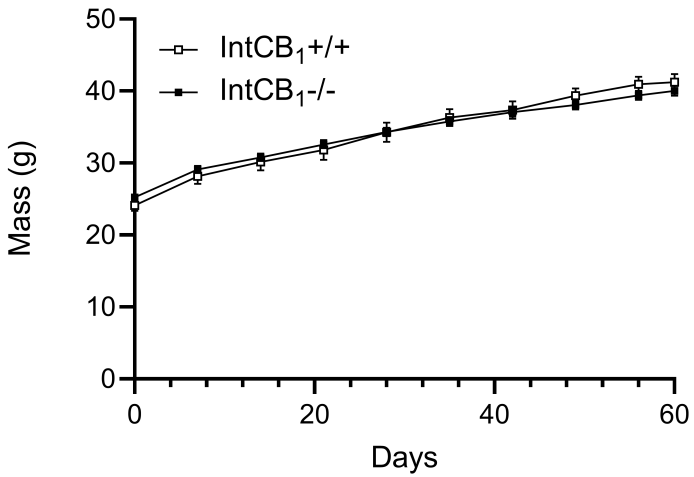
A IntCB₁^{+/+} Western Diet Intake



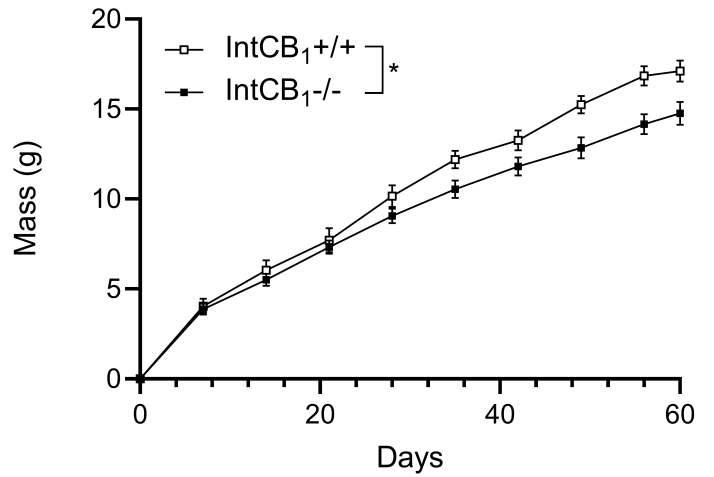
B IntCB₁^{-/-} Western Diet Intake



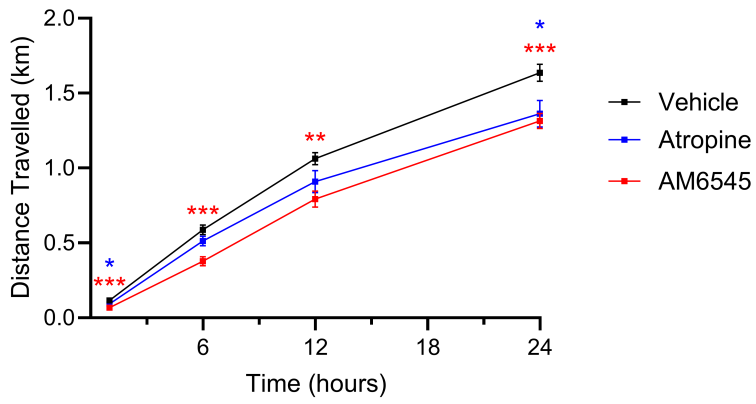
C Body Mass



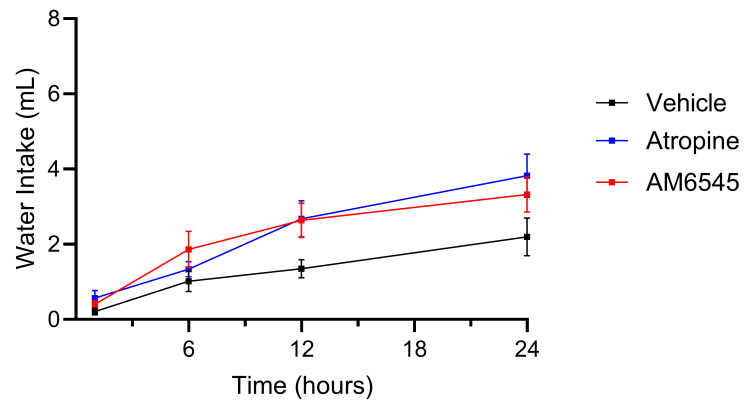
D Body Mass



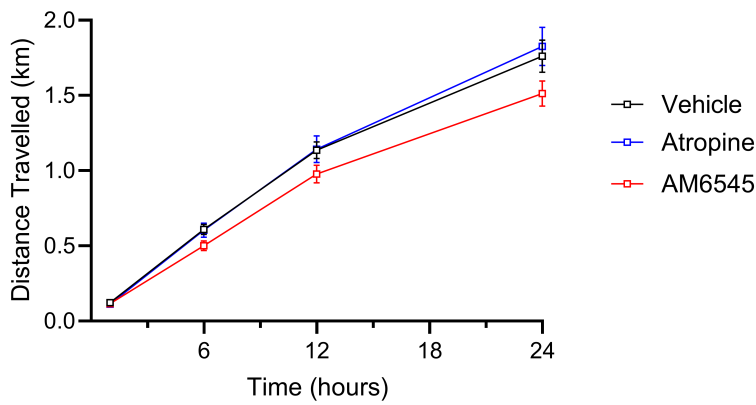
A IntCB₁^{+/+} Distance Travelled Across Time



B IntCB₁^{+/+} Water Intake Across Time



C IntCB₁^{-/-} Distance Travelled Across Time



D IntCB₁^{-/-} Water Intake Across Time

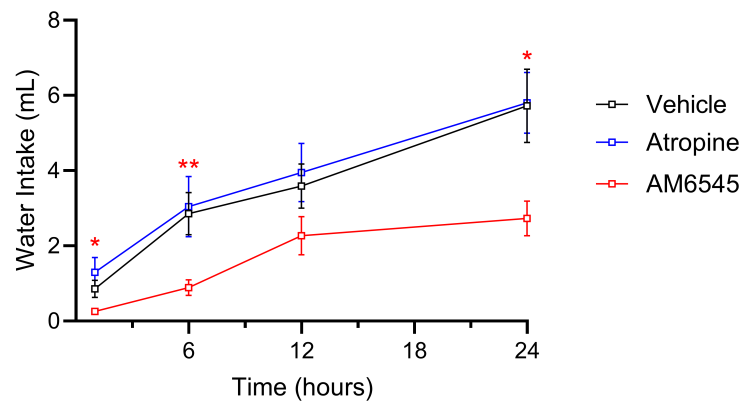


Table 1, 2-Way ANOVA table

Figure	Factor	F (DFn, DFd)	P value	Multiple Comparisons
A	Time	F (1.370, 75.35) = 756.4	<u>P<0.0001</u>	n/a
	Drug	F (3, 55) = 5.875	<u>P=0.0015</u>	1 hr: Vehicle vs. ATR p = 0.0107, Vehicle vs. AM6545 p = 0.0020, Vehicle vs. both p < 0.0001; 6 hr: Vehicle vs. AM6545 p = 0.0020, Vehicle vs. Both p = 0.000; 12 hr: Vehicle vs. AM6545 p = 0.0392, Vehicle vs. Both p = 0.0002
	Time x Drug	F (9, 165) = 1.851	P=0.0628	n/a
B	Time	F (1.576, 83.01) = 95.51	<u>P<0.0001</u>	n/a
	Drug	F (3, 54) = 0.6320	P=0.5957	n/a
	Time x Drug	F (9, 158) = 0.6299	P=0.7703	n/a
C	Time	F (1.119, 61.57) = 344.2	<u>P<0.0001</u>	n/a
	Drug	F (3, 56) = 7.496	<u>P=0.0003</u>	1 hr: Vehicle vs. Both p = 0.0002; 6 hr: Vehicle vs. Both p < 0.0001; 12 hr: Vehicle vs. AM6545 p = 0.0061, Vehicle vs. Both p < 0.0001; 24 hr: Vehicle vs. Both p < 0.0001
	Time x Drug	F (9, 165) = 2.268	P=0.0202	n/a
D	Time	F (1.617, 86.79) = 131.9	<u>P<0.0001</u>	n/a
	Drug	F (3, 56) = 0.9563	P=0.4156	n/a

	Time x Drug	$F(9, 161) = 0.5702$	$P=0.8201$	n/a
E	Time	$F(1.435, 39.70) = 568.4$	<u>$P<0.0001$</u>	n/a
	Drug	$F(1, 28) = 1.086$	$P=0.3063$	n/a
	Time x Drug	$F(3, 83) = 0.5128$	$P=0.6746$	n/a
F	Time	$F(1.632, 42.97) = 44.24$	<u>$P<0.0001$</u>	n/a
	Drug	$F(1, 28) = 5.920$	<u>$P=0.0216$</u>	n/a
	Time x Drug	$F(3, 79) = 3.963$	<u>$P=0.0110$</u>	n/a
G	Time	$F(2.070, 46.91) = 443.1$	<u>$P<0.0001$</u>	n/a
	Drug	$F(1, 24) = 0.3746$	$P=0.5462$	n/a
	Time x Drug	$F(3, 68) = 0.5729$	$P=0.6347$	n/a
H	Time	$F(1.455, 33.47) = 46.34$	<u>$P<0.0001$</u>	n/a
	Drug	$F(1, 24) = 0.4416$	$P=0.5127$	n/a
	Time x Drug	$F(3, 69) = 0.5618$	$P=0.6420$	n/a
I	Time	$F(1.377, 38.10) = 456.1$	<u>$P<0.0001$</u>	n/a
	Drug	$F(1, 28) = 2.280$	$P=0.1423$	n/a
	Time x Drug	$F(3, 83) = 0.4852$	$P=0.6935$	n/a
J	Time	$F(1.587, 40.73) = 147.1$	<u>$P<0.0001$</u>	n/a

	Drug	$F(1, 27) = 1.323$	$P=0.2601$	n/a
	Time x Drug	$F(3, 77) = 0.4454$	$P=0.7212$	n/a
K	Time	$F(1.643, 43.27) = 576.4$	<u>$P<0.0001$</u>	n/a
	Drug	$F(1, 28) = 0.2601$	$P=0.6141$	n/a
	Time x Drug	$F(3, 79) = 0.2981$	$P=0.8267$	n/a
L	Time	$F(1.421, 36.94) = 108.9$	<u>$P<0.0001$</u>	n/a
	Drug	$F(1, 27) = 0.2764$	$P=0.6033$	n/a
	Time x Drug	$F(3, 78) = 0.1415$	$P=0.9348$	n/a

Table 2, 2-Way ANOVA table

Figure	Factor	F (DFn, DFd)	P value	Multiple Comparisons
A	Time	F (1.702, 48.23) = 1085	<u>P<0.0001</u>	n/a
	Drug	F (2, 30) = 6.958	<u>P=0.0033</u>	1 hr: Vehicle vs. AM6545 p = 0.0002, Vehicle vs. ATR p = 0.0455, 6 hr: Vehicle vs. AM6545 p = 0.0002, 12 hr: Vehicle vs. AM6545 p = 0.0025, 24 hr: Vehicle vs. AM6545 p = 0.0008, Vehicle vs. ATR p = 0.0195
	Time x Drug	F (6, 85) = 4.619	<u>P=0.0004</u>	n/a
B	Time	F (1.292, 56.85) = 616.7	<u>P<0.0001</u>	n/a
	Drug	F (2, 45) = 2.272	P=0.1148	n/a
	Time x Drug	F (6, 132) = 2.082	P=0.0595	n/a
C	Time	F (2.130, 58.94) = 74.59	<u>P<0.0001</u>	n/a
	Drug	F (2, 29) = 2.217	P=0.1271	n/a
	Time x Drug	F (6, 83) = 1.707	P=0.1296	n/a
D	Time	F (1.849, 80.75) = 68.67	<u>P<0.0001</u>	n/a
	Drug	F (2, 45) = 3.398	<u>P=0.0422</u>	1 hr: Vehicle vs. AM6545 p = 0.0493, 6 hr: Vehicle vs. AM6545 p = 0.0081, 24 hr: Vehicle vs. AM6545 p = 0.0230
	Time x Drug	F (6, 131) = 2.619	<u>P=0.0197</u>	n/a